2016

3D Hydrodynamic Model Development and Verification

Hussein A. M. Al-Zubaidi
Portland State University

Recommended Citation

Al-Zubaidi, Hussein A. M., "3D Hydrodynamic Model Development and Verification" (2016). *Civil and Environmental Engineering Master's Project Reports*. 25.
https://doi.org/10.15760/CEEMP.6

3D Hydrodynamic Model Development and Verification

BY

HUSSEIN A. M. AL-ZUBAIDI

A research project report submitted in partial fulfillment
of the requirement for the degree of

MASTER OF SCIENCE
IN
CIVIL AND ENVIRONMENTAL ENGINEERING

Project Advisor:
Dr. Scott A. Wells

Portland State University

ACKNOWLEDGMENTS

I would like to express the deepest appreciation to my advisor Dr. Scott Wells who has been aiding and assisting me doing this research project.

I would like to also extend my acknowledgement to my sponsor, Iraq Ministry of Higher Education and Scientific Research (MoHESR) / University of Babylon.

Furthermore, none of this would have been possible without the unconditional love, endless support and extraordinary encouragement of my mother and wife.

ABSTRACT

A three-dimensional numerical model was developed to simulate hydrodynamic, temperature, and water quality distributions in rivers and lakes. In an attempt to get rid of the extra approximation and complexity, no coordinate transformation has been done and z-coordinate system has been employed. The governing equations are the continuity equation, free surface equation, momentum equations, and conservation equations of temperature and water quality. The model employs the time splitting technique which allows splitting the directions in which we end with two-dimensional governing equations and eventually the solution ends with a tri-diagonal matrix, which is easily solved by Thomas algorithm. The first step after developing a numerical model and before adding more features or applying the model to a real case, the model should be verified. The verification of the model was done by implementing the model to known solutions test cases in additional to evaluating whether the code preserves fluid mass. A series of test cases is performed by comparing the model results with the analytical solutions as proposed by many modelers. The model showed good agreement between the analytical and the numerical solution.

TABLE OF CONTENTS

LIST OF FIGURES

1 INTRODUCTION

1.1 Literature review

Many 3D hydrodynamic and water quality models have been developed since 1960s. Different solution techniques have been used to solve the governing equations depending on the model complexity such as finite differences, finite volume, and finite elements approaches. In this work, we consider the finite differences technique to solve the governing equations. The main restriction in developing any model is the computation time which is related to the finite differences scheme. Thus, each approach has its advantages and disadvantages. Also, each model has been tested either by comparing with the analytical solution or with field data or both. Here is a brief description of some well-known three dimensional models.

Blumberg and Mellor (1987) developed a three-dimensional numerical model for estuarine and coastal ocean circulation. The model is based on vertical σ-coordinate and solves the continuity equation, free surface equation, Reynolds momentum equations, and conservation equations of temperature and salinity. The turbulent closure that was proposed by Mellor and Yamada (1982) was used to obtain the vertical kinematic viscosity and diffusivity, while the horizontal viscosity was calculated according to Smagorinsky (1963). Also, the state equation that was given by Fofonoff (1962) was used to calculate the density from temperature and salinity. A mode splitting finite differences technique based on staggered grids was used to solve the governing equations together with their boundary conditions, wind shear stresses at the surface and bottom shear stresses at the bottom. The mode splitting technique separates the governing equations into an external and internal mode. In the external mode, shallow water wave equations are obtained by integrating the governing equations vertically and then solved explicitly in a short time step to satisfy gravity wave CFL limitation. The free surface elevation resulted from the external mode is then used to solve the internal mode, original governing equations, in a long time step independently from the external mode by treating just the vertical diffusion terms implicitly. This technique helps the stability of the internal mode to not be affected by the gravity wave stability, leading to much longer time step than the internal mode. Finally, the internal mode produces tri-diagonal system of linear equations which are then solved by Gaussian elimination method. Different experiments were done for testing the model performance. In a 2-1/2-day experiments

with 32*km*×24*km*, 16 vertical layers of different depths, and 144 time step/day, it took 1*min*/*day* on a Cray-1s computer.

This model has been developed by several authors since 1987 when the original model later became the POM, the Princeton Ocean Model (Mellor 2003). In the late 1990s and the 2000s, many three dimensional models have been derived from POM such as ECOM, NCOM, and FVCOM.

Hamrick (1992) developed the Environmental Fluid Dynamic Code, EFDC, which is a three-dimensional model equivalent to Blumberg and Mellor (1987) in its physics and many aspects of the computational scheme. The main differences between the two models are the internal and external mode solution of EFDC model is at the same time step, and EFDC model implements a number of alternate advection schemes. A further development of EFDC model leads EFDC-Hydro, a special version developed for U.S. EPA Region 4 (Tetra Tech 2002). About the model verification, it is done by comparing the numerical solution with observed data and calculating the error.

Casulli and Cheng (1992) developed the first phase of a three-dimensional numerical model for shallow water flow (TRIM-3D). The governing equations were derived from Navier-Stokes equations based on turbulent averaging and assuming a constant density and hydrostatic pressure. The non-conservative forms of vertically averaged horizontal and vertical momentum equations, free surface equation, and continuity equation were solved in conjugate with dry/flood conditions and without coordinate transformations. Moreover, wind and bottom stresses were included in momentum equations. The numerical solution was based on fixed staggered grids with a semi-implicit finite differences method and used Eulerian-Lagrangian method for treating the convective terms in additional to treating vertical diffusion terms implicitly and horizontal diffusion terms explicitly. The model stability condition depended on horizontal viscosity. The numerical solution of this model yields two types of linear systems, tri-diagonal from the numerical solution of the horizontal velocities and penta-diagonal from the numerical solution of the free surface equation. The model was verified and calibrated by implementing it on two different case studies. In one of these cases, Lagoon of Venice in Italy was simulated for 12*hrs* with horizontal mesh dimensions of 100*m*×100*m*, time step of 15*min*, and 10 vertical layers are set at different depths. It took only 134 CPU *seconds* on Cray Y-MP8/432. Also, Casulli and Walters (2000) developed an unstructured grid version of this model, UnTRIM.

Different models have been developed based on the model of Casulli and Cheng (1992) . The most well-known is ELCOM. Hodges and Dallimore (2006) developed the estuary, lake and coastal ocean model (ELCOM), a three-dimensional model used to simulate hydrodynamics and water quality in surface waters. The fundamental numerical scheme was based on the model developed by Casulli and Cheng (1992) with some adjustments relevant to accuracy, scalar conservation, numerical diffusion, a new option for calculating vertical turbulent fluxes by application of a mixed-layer turbulence closure scheme. Using the mixed-layer scheme eliminates solving a tri-diagonal matrix for each water column. Whereas the advection terms in hydrodynamic equations were treated similar to TRIM model, a conservative third-order scalar transport method (ULTIMATE QUICKEST) was used.

Ahsan and Blumberg (1999) developed a three-dimensional numerical model for simulating the dynamic and thermal distribution in Onondaga Lake, New York. This model, called ECOMsiz, was another version of Blumberg and Mellor (1987) model, called ECOM. ECOMsiz employs z-coordinate system and uses semi-implicit finite differences method similar to that was developed by Casulli and Cheng (1992). Thus, the stability condition depends only on the horizontal viscosity and the solution scheme of the convective terms if they discretized explicitly. Moreover, surface heat exchange was included in this work and based on bulk formulas reported in Buchak and Cole (1995). Two years of data, 1985 and 1989, were used to calibrate and validate ECOMsiz.

Another way to eliminate the stability related to gravity waves and provide a long time step for a large scale current system economically was illustrated in Bryan (1969) in which gravity waves are filtered out of the solution by using a “rigid-lid” approximation. For oceans circulation, this method is still adequate, but for lakes under variable wind in space and time it did not reproduce realistic results (Smith 2006).

Wang and Falconer (1998) simulated the flow and disinfection processes in disinfection contact tanks by developing a three-dimensional model. Reynolds-averaged equations of continuity and momentums were integrated vertically and then free and bottom boundary conditions and different turbulent closure models were applied. The numerical solution based on a time marching method which was alternating-directions-implicit scheme. In an attempt to remove the numerical diffusion resulting from using a first order accurate upwind scheme, higher order upwind schemes (QUICK and a third order upwind scheme) were used in additional to the first

order accurate scheme. This model was validated and investigated by comparing model results with physical model tank results. The mesh consisted of 49×24 grids spaces with a spatial resolution of 0.043×0.042m. An initial time step of 0.15s, based on average gravity Courant number of 8, was used to start the computations till the initial disturbance had finished and a steady state velocity distribution was obtained. Various combinations of turbulent closure models and upwind schemes were investigated. The results showed that each combination has advantages and disadvantages relevant to chlorine contact tanks.

1.2 Scope and Objectives

The main purpose of this paper is to validate and evaluate the hydrodynamic results of a new 3D hydrodynamic model by doing a series of test cases. Also, we will introduce the effects of the time step and the gravity wave speed on the wave damping that is resulting from the use of this numerical scheme.

2 MODEL DESCRIPTION

2.1 Hydrodynamic governing equations

The three dimensional hydrodynamic governing equations are derived from the Navier-Stokes equations. After averaging the Navier-Stokes equations, we obtain the Reynolds-averaged equations, which are as follows:

Continuity Equation:

$$\frac{\partial \rho}{\partial t} + \frac{\partial \rho \bar{u}}{\partial x} + \frac{\partial \rho \bar{v}}{\partial y} + \frac{\partial \rho \bar{w}}{\partial z} = 0$$

Where: $\bar{u}, \bar{v}, and\ \bar{w}$ are the average velocities in the *x*, *y*, and *z* directions, respectively, and ρ is the density.

Momentum Equations:

X-Momentum: $$\frac{d\rho\bar{u}}{dt} + \rho f_* \bar{w} - \rho f \bar{v} = -\frac{\partial \bar{p}}{\partial x} + \frac{\partial(\tau^{xx} + \tau_{xx})}{\partial x} + \frac{\partial(\tau^{xy} + \tau_{xy})}{\partial y} + \frac{\partial(\tau^{xz} + \tau_{xz})}{\partial z}$$

Y-Momentum: $$\frac{d\rho\bar{v}}{dt} + \rho f \bar{u} = -\frac{\partial \bar{p}}{\partial y} + \frac{\partial(\tau^{yx} + \tau_{yx})}{\partial x} + \frac{\partial(\tau^{yy} + \tau_{yy})}{\partial y} + \frac{\partial(\tau^{yz} + \tau_{yz})}{\partial z}$$

Z-Momentum: $$\frac{d\rho\bar{w}}{dt} - \rho f_* \bar{u} = -\frac{\partial \bar{p}}{\partial z} - \rho g + \frac{\partial(\tau^{zx} + \tau_{zx})}{\partial x} + \frac{\partial(\tau^{zy} + \tau_{zy})}{\partial y} + \frac{\partial(\tau^{zz} + \tau_{zz})}{\partial z}$$

The material derivative $\frac{d}{dt}$ includes the time rate of change and the advective terms:

$$\frac{d}{dt} = \frac{\partial}{\partial t} + \bar{u}\frac{\partial}{\partial x} + \bar{v}\frac{\partial}{\partial y} + \bar{w}\frac{\partial}{\partial z}$$

Where:

$f = 2\Omega \sin\varphi$, called Coriolis parameter (positive above the equator, zero at the equator, and negative under the equator),

$f_* = 2\Omega \cos\varphi$, called reciprocal Coriolis parameter (positive in both hemispheres and approaches to zero at the poles),

Ω = rotation rate of the earth,

φ = the latitude,

p = pressure,

g = gravitational acceleration.

τ^{xx}, τ^{xy}, and τ^{xz} = viscous shear stresses, and

τ_{xx}, τ_{xy}, and τ_{xz} = turbulent shear stresses or Reynolds stresses..

2.2 Coordinates system

In this work, we assume the coordinate system is as shown in Figure 1. The x-axis is at the free water surface, positive to the right in the flow direction, the y-axes is also at the free water surface, and z-axis is the vertical axis, positive downward. $\propto$ is the slope of water body, which is the channel slope.

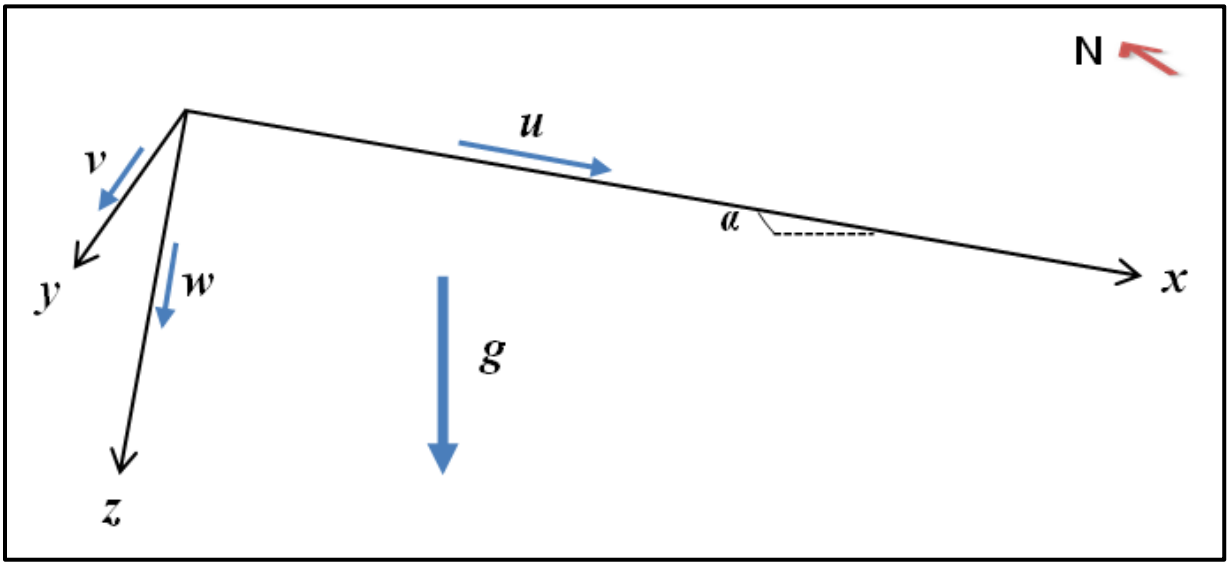

Figure 1: Positive direction coordinate system

Assuming there is no change in the bottom elevation, *h*, with y-axis ($\frac{\partial h}{\partial y} = 0$), the gravitational acceleration, g, can be analysis into two components. These components increase the momentum in the x and z direction. Thus, one of these components is in the x-axis direction, and the other is in the z-axis direction.

$$g_x = -g\frac{\partial h}{\partial x} = g\sin\alpha$$

$$g_z = -g\frac{\partial h}{\partial z} = g\cos\alpha$$

2.3 Hydrodynamic governing equations simplification

2.3.1 Assumptions

We will make the following assumptions:

- Incompressible fluid.
- Centripetal acceleration is ignored.
- Boussinesq approximation.
- $\rho = \rho_\circ + \Delta\rho = \rho_\circ$ where $\rho_\circ$ is the base density and $\Delta\rho$ represents the variation of $\rho_\circ$ with time.
- Neglect the reciprocal Coriolis parameter ($f_* = 2\Omega\cos\varphi$).
- Neglect the viscous shear stresses except at the boundaries where the turbulent shear stresses goes to zero.

Applying all the assumptions to the continuity and momentum equations and rearrange the terms, we get turbulent time-averaged equations:

The continuity equation:

$$\frac{\partial\bar{u}}{\partial x} + \frac{\partial\bar{v}}{\partial y} + \frac{\partial\bar{w}}{\partial z} = 0$$

X-Momentum:

$$\frac{\partial\bar{u}}{\partial t} + \bar{u}\frac{\partial\bar{u}}{\partial x} + \bar{v}\frac{\partial\bar{u}}{\partial y} + \bar{w}\frac{\partial\bar{u}}{\partial z} = -\frac{1}{\rho_\circ}\frac{\partial\bar{p}}{\partial x} + f\bar{v} + \frac{1}{\rho_\circ}\frac{\partial(\tau_{xx})}{\partial x} + \frac{1}{\rho_\circ}\frac{\partial(\tau_{xy})}{\partial y} + \frac{1}{\rho_\circ}\frac{\partial(\tau_{xz})}{\partial z}$$

Y-Momentum:

$$\frac{\partial\bar{v}}{\partial t} + \bar{u}\frac{\partial\bar{v}}{\partial x} + \bar{v}\frac{\partial\bar{v}}{\partial y} + \bar{w}\frac{\partial\bar{v}}{\partial z} = -\frac{1}{\rho_\circ}\frac{\partial\bar{p}}{\partial y} - f\bar{u} + \frac{1}{\rho_\circ}\frac{\partial(\tau_{yx})}{\partial x} + \frac{1}{\rho_\circ}\frac{\partial(\tau_{yy})}{\partial y} + \frac{1}{\rho_\circ}\frac{\partial(\tau_{yz})}{\partial z}$$

Z-Momentum:

$$\frac{\partial\bar{w}}{\partial t} + \bar{u}\frac{\partial\bar{w}}{\partial x} + \bar{v}\frac{\partial\bar{w}}{\partial y} + \bar{w}\frac{\partial\bar{w}}{\partial z} = -\frac{1}{\rho_\circ}\frac{\partial\bar{p}}{\partial z} - \frac{\rho g}{\rho_\circ} + \frac{1}{\rho_\circ}\frac{\partial(\tau_{zx})}{\partial x} + \frac{1}{\rho_\circ}\frac{\partial(\tau_{zy})}{\partial y} + \frac{1}{\rho_\circ}\frac{\partial(\tau_{zz})}{\partial z}$$

2.3.2 Reynolds stresses

Reynolds stresses can be written in the simplest approach in *i*, and *j* notation form as follows:

$$\frac{\tau_{ij}}{\rho_\circ} = -u_i'u_j' = \upsilon_{tj}\frac{\partial u_i}{\partial x_j}$$

Where:

u_i = velocity component in the *i* direction.

u' = the fluctuation of the velocity component.

j = 1, 2, and 3 are the coordinate system *x*, *y*, and *z*, respectively.

υ_{tj} = turbulent kinematic viscosity in the *j* direction.

If we substitute the Reynolds stresses in the momentum equations and if we recognize two kinds of turbulent kinematic viscosities in the horizontal and vertical directions, the momentum equations in the three directions can be written as follows:

X-Momentum:

$$\frac{\partial \bar{u}}{\partial t} + \bar{u}\frac{\partial \bar{u}}{\partial x} + \bar{v}\frac{\partial \bar{u}}{\partial y} + \bar{w}\frac{\partial \bar{u}}{\partial z} = -\frac{1}{\rho_\circ}\frac{\partial \bar{p}}{\partial x} + f\bar{v} + \frac{\partial}{\partial x}\left[\upsilon_h \frac{\partial \bar{u}}{\partial x}\right] + \frac{\partial}{\partial y}\left[\upsilon_h \frac{\partial \bar{u}}{\partial y}\right] + \frac{\partial}{\partial z}\left[\upsilon_v \frac{\partial \bar{u}}{\partial z}\right]$$

Y-Momentum:

$$\frac{\partial \bar{v}}{\partial t} + \bar{u}\frac{\partial \bar{v}}{\partial x} + \bar{v}\frac{\partial \bar{v}}{\partial y} + \bar{w}\frac{\partial \bar{v}}{\partial z} = -\frac{1}{\rho_\circ}\frac{\partial \bar{p}}{\partial y} - f\bar{u} + \frac{\partial}{\partial x}\left[\upsilon_h \frac{\partial \bar{v}}{\partial x}\right] + \frac{\partial}{\partial y}\left[\upsilon_h \frac{\partial \bar{v}}{\partial y}\right] + \frac{\partial}{\partial z}\left[\upsilon_v \frac{\partial \bar{v}}{\partial z}\right]$$

Z-Momentum:

$$\frac{\partial \bar{w}}{\partial t} + \bar{u}\frac{\partial \bar{w}}{\partial x} + \bar{v}\frac{\partial \bar{w}}{\partial y} + \bar{w}\frac{\partial \bar{w}}{\partial z} = -\frac{1}{\rho_\circ}\frac{\partial \bar{p}}{\partial z} - \frac{\rho g}{\rho_\circ} + \frac{\partial}{\partial x}\left[\upsilon_h \frac{\partial \bar{w}}{\partial x}\right] + \frac{\partial}{\partial y}\left[\upsilon_h \frac{\partial \bar{w}}{\partial y}\right] + \frac{\partial}{\partial z}\left[\upsilon_v \frac{\partial \bar{w}}{\partial z}\right]$$

Where: υ_h is the horizontal turbulent kinematic viscosity, and υ_v is the vertical turbulent kinematic viscosity.

2.3.3 Gravitational acceleration components

Adding the two components of the gravitational acceleration to the momentum equations, the equations will be as follows:

X-Momentum:

$$\frac{\partial \bar{u}}{\partial t} + \bar{u}\frac{\partial \bar{u}}{\partial x} + \bar{v}\frac{\partial \bar{u}}{\partial y} + \bar{w}\frac{\partial \bar{u}}{\partial z} = -\frac{1}{\rho_\circ}\frac{\partial \bar{p}}{\partial x} + f\bar{v} + g\sin\alpha + \frac{\partial}{\partial x}\left[\upsilon_h \frac{\partial \bar{u}}{\partial x}\right] + \frac{\partial}{\partial y}\left[\upsilon_h \frac{\partial \bar{u}}{\partial y}\right] + \frac{\partial}{\partial z}\left[\upsilon_v \frac{\partial \bar{u}}{\partial z}\right]$$

Y-Momentum:

$$\frac{\partial \bar{v}}{\partial t}+\bar{u}\frac{\partial \bar{v}}{\partial x}+\bar{v}\frac{\partial \bar{v}}{\partial y}+\bar{w}\frac{\partial \bar{v}}{\partial z}=-\frac{1}{\rho_{\circ}}\frac{\partial \bar{p}}{\partial y}-f\bar{u}+\frac{\partial}{\partial x}\left[\upsilon_h\frac{\partial \bar{v}}{\partial x}\right]+\frac{\partial}{\partial y}\left[\upsilon_h\frac{\partial \bar{v}}{\partial y}\right]+\frac{\partial}{\partial z}\left[\upsilon_v\frac{\partial \bar{v}}{\partial z}\right]$$

Z-Momentum:

$$\frac{\partial \bar{w}}{\partial t}+\bar{u}\frac{\partial \bar{w}}{\partial x}+\bar{v}\frac{\partial \bar{w}}{\partial y}+\bar{w}\frac{\partial \bar{w}}{\partial z}=-\frac{1}{\rho_{\circ}}\frac{\partial \bar{p}}{\partial z}+\frac{\rho g}{\rho_{\circ}}\cos\alpha+\frac{\partial}{\partial x}\left[\upsilon_h\frac{\partial \bar{w}}{\partial x}\right]+\frac{\partial}{\partial y}\left[\upsilon_h\frac{\partial \bar{w}}{\partial y}\right]+\frac{\partial}{\partial z}\left[\upsilon_v\frac{\partial \bar{w}}{\partial z}\right]$$

2.3.4 The hydraulic assumption

When horizontal accelerations are larger than vertical accelerations, a scaling analysis of the z-momentum equation shows that, all terms can be cancelled except the first and second term in the right side of the equation. Thus, the z-momentum equation will be written in a new form:

$$0=-\frac{1}{\rho_{\circ}}\frac{\partial \bar{p}}{\partial z}+\frac{\rho g}{\rho_{\circ}}\cos\alpha$$

Solving this first order differential equation leads to the following equation:

$$\bar{p}=\overline{p_a}+g\cos\alpha\int_{\eta}^{z}\rho dz$$

Where: η is the free surface elevation, and p_a is the atmospheric pressure at the free surface elevation.

By deriving the pressure equation with respect to *x* and *y*, and applying Leibnitz's rule, we get a new expression to the pressure term in x and y-momentum equation:

$$\frac{\partial \bar{p}}{\partial x}=\frac{\partial \overline{p_a}}{\partial x}+g\cos\alpha\int_{\eta}^{z}\frac{\partial \rho}{\partial x}dz-\rho g\cos\alpha\frac{\partial \eta}{\partial x}$$

$$\frac{\partial \bar{p}}{\partial y}=\frac{\partial \overline{p_a}}{\partial y}+g\cos\alpha\int_{\eta}^{z}\frac{\partial \rho}{\partial y}dz-\rho g\cos\alpha\frac{\partial \eta}{\partial y}$$

Assuming there is no change in the atmospheric pressure ($\frac{\partial \overline{p_a}}{\partial x}=\frac{\partial \overline{p_a}}{\partial y}=0$), and after substituting the pressure terms in x and y-momentum equation, we obtain

X-Momentum:

$$\frac{\partial \bar{u}}{\partial t}+\bar{u}\frac{\partial \bar{u}}{\partial x}+\bar{v}\frac{\partial \bar{u}}{\partial y}+\bar{w}\frac{\partial \bar{u}}{\partial z}=g\cos\alpha\frac{\partial \eta}{\partial x}-\frac{g\cos\alpha}{\rho_{\circ}}\int_{\eta}^{z}\frac{\partial \rho}{\partial x}dz+f\bar{v}+g\sin\alpha$$
$$+\frac{\partial}{\partial x}\left[\upsilon_h\frac{\partial \bar{u}}{\partial x}\right]+\frac{\partial}{\partial y}\left[\upsilon_h\frac{\partial \bar{u}}{\partial y}\right]+\frac{\partial}{\partial z}\left[\upsilon_v\frac{\partial \bar{u}}{\partial z}\right]$$

Y-Momentum:

$$\frac{\partial \bar{v}}{\partial t}+\bar{u}\frac{\partial \bar{v}}{\partial x}+\bar{v}\frac{\partial \bar{v}}{\partial y}+\bar{w}\frac{\partial \bar{v}}{\partial z}=g\cos\alpha\frac{\partial \eta}{\partial y}-\frac{g\cos\alpha}{\rho_{\circ}}\int_{\eta}^{z}\frac{\partial \rho}{\partial y}dz-f\bar{u}$$
$$+\frac{\partial}{\partial x}\left[\upsilon_h\frac{\partial \bar{v}}{\partial x}\right]+\frac{\partial}{\partial y}\left[\upsilon_h\frac{\partial \bar{v}}{\partial y}\right]+\frac{\partial}{\partial z}\left[\upsilon_v\frac{\partial \bar{v}}{\partial z}\right]$$

The hydrostatic pressure:

$$\frac{\partial \bar{p}}{\partial z}=\rho g\cos\alpha$$

2.3.5 Lateral discharge

We will assume that additional momentum from the lateral tributaries causes shear stresses in the longitudinal and lateral direction. These shear stresses can be added to the main momentum equations. If we assume the tributaries inter the main stream as shown in Figure 2, the main velocity of the tributary that enter the main stream can be analysis into two components:

$$u_x = u cos\beta$$
$$u_y = u sin\beta$$

Where:

u_x = longitudinal velocity component of the tributary in x-direction of the main stream.

u_y = lateral velocity component of the tributary velocity in y-direction of the main stream.

β = the angle between the main stream and the tributary as shown in Figure 2.

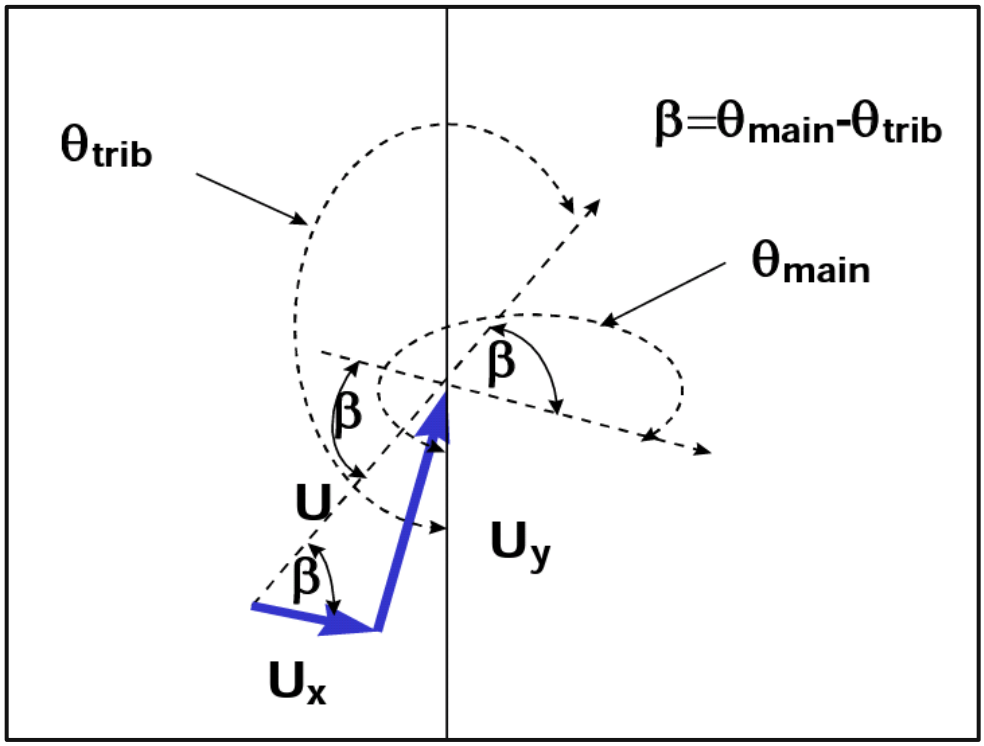

Figure 2: Lateral discharge

Now, the momentum equations become as follows after adding the two lateral velocities:

X-Momentum:

$$\frac{\partial \bar{u}}{\partial t}+\bar{u}\frac{\partial \bar{u}}{\partial x}+\bar{v}\frac{\partial \bar{u}}{\partial y}+\bar{w}\frac{\partial \bar{u}}{\partial z}=g\cos\alpha\frac{\partial \eta}{\partial x}-\frac{g\cos\alpha}{\rho_{\circ}}\int_{\eta}^{z}\frac{\partial \rho}{\partial x}dz+f\bar{v}+g\sin\alpha$$
$$+\frac{\partial}{\partial x}\left[\upsilon_h\frac{\partial \bar{u}}{\partial x}\right]+\frac{\partial}{\partial y}\left[\upsilon_h\frac{\partial \bar{u}}{\partial y}\right]+\frac{\partial}{\partial z}\left[\upsilon_v\frac{\partial \bar{u}}{\partial z}\right]+qu_x$$

Y-Momentum:

$$\frac{\partial \bar{v}}{\partial t}+\bar{u}\frac{\partial \bar{v}}{\partial x}+\bar{v}\frac{\partial \bar{v}}{\partial y}+\bar{w}\frac{\partial \bar{v}}{\partial z}=g\cos\alpha\frac{\partial \eta}{\partial y}-\frac{g\cos\alpha}{\rho_{\circ}}\int_{\eta}^{z}\frac{\partial \rho}{\partial y}dz-f\bar{u}$$
$$+\frac{\partial}{\partial x}\left[\upsilon_h\frac{\partial \bar{v}}{\partial x}\right]+\frac{\partial}{\partial y}\left[\upsilon_h\frac{\partial \bar{v}}{\partial y}\right]+\frac{\partial}{\partial z}\left[\upsilon_v\frac{\partial \bar{v}}{\partial z}\right]+qu_y$$

Where:

q = The lateral discharge per unit volume.

2.3.6 Free surface equation:

The free surface equation can be derived by integrating the continuity equation over the total depth (see Figure 3 for free surface integration limits) and applying kinematic boundary conditions derived from a mass balance at the surface and bottom layer of the water body.

$$\frac{\partial \eta}{\partial t} = \frac{\partial}{\partial x}\int_{\eta}^{h} \bar{u}\,dz + \frac{\partial}{\partial y}\int_{\eta}^{h} \bar{v}\,dz - \int_{\eta}^{h} q\,dz$$

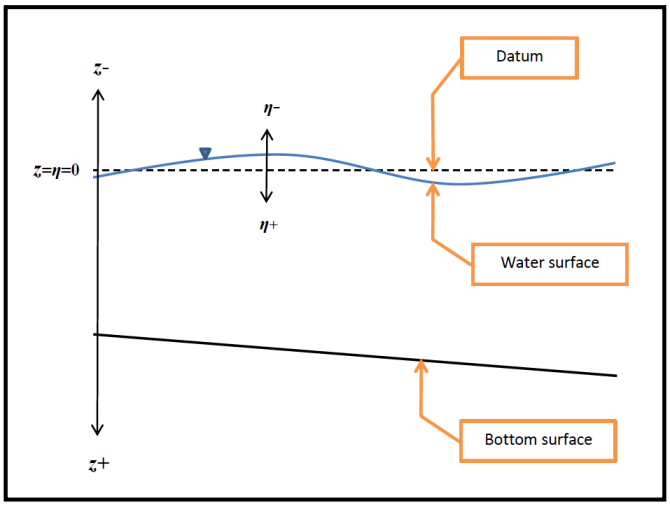

Figure 3: Free surface integration limits

2.4 Heat and water quality transport governing equation

Heat and water quality transport are governed by the advection diffusion equation which can be written in a general form as follows:

$$\frac{\partial \phi}{\partial t} + \frac{\partial \bar{u}\phi}{\partial x} + \frac{\partial \bar{v}\phi}{\partial y} + \frac{\partial \bar{w}\phi}{\partial z} = \frac{\partial}{\partial x}\left[D_h \frac{\partial \phi}{\partial x}\right] + \frac{\partial}{\partial y}\left[D_h \frac{\partial \phi}{\partial y}\right] + \frac{\partial}{\partial z}\left[D_v \frac{\partial \phi}{\partial z}\right] + S_\phi$$

Where:

$\boldsymbol{\phi}$ is the constituent concentration (g/m^3)

S_ϕ is the source/sink term of the constituent ϕ (g/m^3/sec), and

D_h and D_v are the horizontal and vertical diffusion confident (diffusivity) (m^2/sec), respectively.

Note that, in case of heat transport, ϕ is determined by converting the energy to mass using the specific heat of water, c_p:

$$\phi = \rho c_p T$$

Where T is the temperature.

2.5 Boundary shear stresses

Surface shear stresses, or wind shear stresses, are connected to the surface boundary conditions ($z = \eta$). These stresses are related to the wind velocity distribution above the water body, as shown in Figure 4, and can be described as follows:

$$\tau_s = \rho_a C_D U|U|$$

Where:

τ_s = The surface shear stress.

ρ_a = The air density.

C_D = The drag coefficient.

$$U = W_h - U_s$$

Where:

W_h = Wind velocity at height *h*, usually h is taken at 10*m* height.

U_s = Surface shear velocity.

Because $W_h \gg U_s$, U is assumed equal to W_h, and the surface shear stresses can be written as follows after analysis the wind velocity into two components:

$$(\tau_{sx}, \tau_{sy}) = \rho_a C_D (W_x, W_y) \sqrt{W_x^2 + W_y^2}$$

Where:

τ_{sx}, and τ_{sy} = Surface shear stresses in the *x*, and *y* direction, respectively.

W_x, and W_y = Wind velocities in in the *x*, and *y* direction, respectively measured at 10*m* height above the free surface elevation. If the available depth is at different height than 10*m*, we can calculate the wind velocity at 10*m* height from the following equation:

$$\frac{W_z}{W_{Z1}} = \frac{\ln\left(\frac{z}{z_\circ}\right)}{\ln\left(\frac{z_1}{z_\circ}\right)}$$

Where:

W_z = Wind velocity at elevation *z*.

W_{Z1} = Wind velocity at elevation z_1.

$Z_\circ$ = Wind roughness height,

= 0.003 for wind velocity less than 5*mph*,

=0.015 for wind velocity greater than 5*mph*.

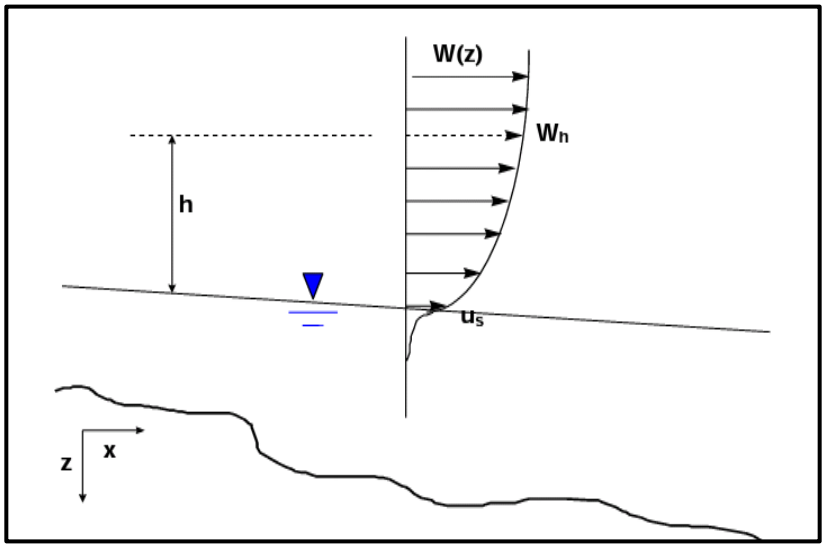

Figure 4: Wind velocity distribution above the free water surface

In addition, the wind shear stresses can be written depending on the angle that wind makes with the northern direction:

$$(\tau_{sx}, \tau_{sy}) = \rho_a C_D W_h^2 (cos\theta, sin\theta)$$

Where:

$$\theta = \theta_1 - \theta_2$$

θ_1 = the angle that wind makes with the northern direction in radians (measured clockwise from the north).

θ_2 = the angle that the segment makes with the northern direction in radians (measured clockwise from the north).

Bottom shear stresses, or wall shear stresses, are connected to the bottom boundary conditions ($z = h$) and can be calculated depending on the horizontal velocities that are just above the bottom from the following equation:

$$\tau_b = \frac{\rho_w g}{C^2} U|U|$$

Where:

τ_b = The bottom shear stress.

ρ_w = The water density.

C = Chezy's coefficient.

Chezy's coefficient is also related to the Manning's coefficient,

$$C = \frac{1}{n} R^{1/6}$$

Where:

n = Manning's coefficient.

R = the hydraulic radius.

Thus, the bottom shear stresses can be written as follows after analyzing velocities into two components:

$$(\tau_{bx}, \tau_{by}) = \frac{\rho_w g}{C^2} (\bar{u}, \bar{v}) \sqrt{\bar{u}^2 + \bar{v}^2}$$

2.6 Numerical solution

2.6.1 The computational grid, physical domain, and the input bathymetry

A staggered grid distribution is used for all variables in the domain as shown in Figure 5. The domain is divided into cells. Each cell is defined at the center by i, j, and k after dividing the domain into cells, an example of the input bathymetry is shown in Figure 5.

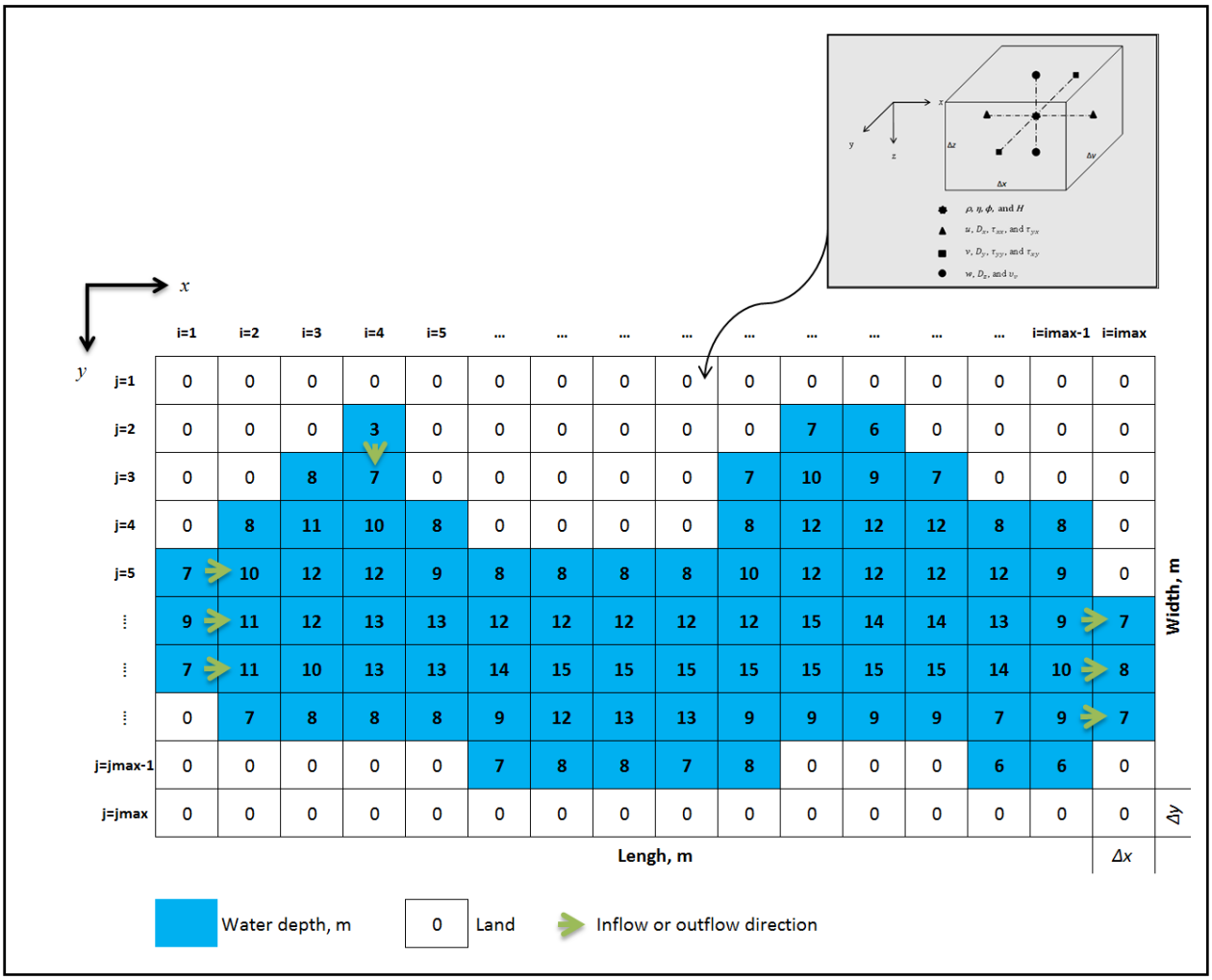

Figure 5: An example of the computational grid, physical domain, and input bathymetry

2.6.2 Numerical solution of the free surface equation

The free water surface equation is solved by substituting the finite difference approximations of x and y-momentum equation into free surface equation.

$$\bar{u}_{i,j,k}^{n+1} = \bar{u}_{i,j,k}^{n} + \Delta t\left[F_x + g\cos\alpha\frac{\partial\eta}{\partial x} - \frac{g\cos\alpha}{\rho_\circ}\int_\eta^z \frac{\partial\rho}{\partial x}dz + \frac{1}{\rho_\circ}\frac{\partial(\tau_{xz})}{\partial z} + qu_x \right]_{i,j,k}^{n}$$

$$\bar{v}_{i,j,k}^{n+1} = \bar{v}_{i,j,k}^{n} + \Delta t\left[F_y + g\cos\alpha\frac{\partial\eta}{\partial y} - \frac{g\cos\alpha}{\rho_\circ}\int_\eta^z \frac{\partial\rho}{\partial y}dz + \frac{1}{\rho_\circ}\frac{\partial(\tau_{yz})}{\partial z} + qu_y \right]_{i,j,k}^{n}$$

Where F_x and F_y are explicit operators that account for the advection, horizontal and vertical turbulent shear stresses, Coriolis, and gravitational acceleration component.

$$F_x = -\bar{u}\frac{\partial\bar{u}}{\partial x} - \bar{v}\frac{\partial\bar{u}}{\partial y} - \bar{w}\frac{\partial\bar{u}}{\partial z} + \frac{1}{\rho_\circ}\frac{\partial(\tau_{xx})}{\partial x} + \frac{1}{\rho_\circ}\frac{\partial(\tau_{xy})}{\partial y} + f\bar{v} + g\sin\alpha$$

$$F_y = -\bar{u}\frac{\partial\bar{v}}{\partial x} - \bar{v}\frac{\partial\bar{v}}{\partial y} - \bar{w}\frac{\partial\bar{v}}{\partial z} + \frac{1}{\rho_\circ}\frac{\partial(\tau_{yx})}{\partial x} + \frac{1}{\rho_\circ}\frac{\partial(\tau_{yy})}{\partial y} - f\bar{u}$$

The advective terms are then converted to finite differences using an upwind scheme.

Substituting $\bar{u}_{i,j,j}^{n+1}$ and $\bar{v}_{i,j,j}^{n+1}$ into free water surface equation for $\bar{u}$ and $\bar{v}$, respectively.

$$\begin{aligned}
\frac{\partial\eta}{\partial t} = {} & \frac{\partial}{\partial x}\int_\eta^h \bar{u}_{i,j,k}^{n}dz + \Delta t\frac{\partial}{\partial x}\int_\eta^h F_x\big|_{i,j,k}^{n}dz + \Delta t\frac{\partial}{\partial x}\int_\eta^h g\cos\alpha\frac{\partial\eta}{\partial x}\Big|_{i,j}^{n}dz - \Delta t\frac{\partial}{\partial x}\int_\eta^h \frac{g\cos\alpha_x}{\rho_\circ}\int_\eta^z\frac{\partial\rho}{\partial x}dz\Big|_{i,j,k}^{n}dz \\
& + \Delta t\frac{\partial}{\partial x}\int_\eta^h \frac{1}{\rho_\circ}\frac{\partial(\tau_{xz})}{\partial z}\Big|_{i,j,k}^{n}dz + \Delta t\frac{\partial}{\partial x}\int_\eta^h q\bar{u}_x\big|_{i,j,k}^{n}dz + \frac{\partial}{\partial y}\int_\eta^h \bar{v}_{i,j,k}^{n}dz + \Delta t\frac{\partial}{\partial y}\int_\eta^h F_y\big|_{i,j,k}^{n}dz \\
& + \Delta t\frac{\partial}{\partial y}\int_\eta^h g\cos\alpha\frac{\partial\eta}{\partial y}\Big|_{i,j}^{n}dz - \Delta t\frac{\partial}{\partial y}\int_\eta^h \frac{g\cos\alpha_y}{\rho_\circ}\int_\eta^z\frac{\partial\rho}{\partial y}dz\Big|_{i,j,k}^{n}dz + \Delta t\frac{\partial}{\partial y}\int_\eta^h \frac{1}{\rho_\circ}\frac{\partial(\tau_{yz})}{\partial z}\Big|_{i,j,k}^{n}dz \\
& + \Delta t\frac{\partial}{\partial y}\int_\eta^h q\bar{u}_y\big|_{i,j,k}^{n}dz - \int_\eta^h q\big|_{i,j,k}^{n}dz
\end{aligned}$$

By defining new variables $H_{rx}\big|_{i,j,k}$ and $H_{ry}\big|_{i,j,k}$,

$$H_{rx}\big|_{i,j,k} = \frac{H\big|_{i,j,k} + H\big|_{i+1,j,k}}{2}$$

$$H_{ry}\big|_{i,j,k} = \frac{H\big|_{i,j,k} + H\big|_{i,j+1,k}}{2}$$

Also, a backward difference is used for the unsteady term,

$$\frac{\partial \eta}{\partial t} = \frac{n_{i,j}^{n} - n_{i,j}^{n-1}}{\Delta t}$$

Simplifying,

$$W\eta_{i-1,j}^{n} + N\eta_{i,j-1}^{n} + C\eta_{i,j}^{n} + +S\eta_{i,j+1}^{n} + E\eta_{i+1,j}^{n} = R$$

Where:

$$W = \left[\frac{-\Delta t^2 \Delta y g \cos\alpha}{\Delta x} \sum_{k=1}^{K} H\Big|_{i-1,j} \right]$$

$$N = \left[\frac{-\Delta t^2 \Delta x g \cos\alpha}{\Delta y} \sum_{k=1}^{K} H\Big|_{i,j-1} \right]$$

$$C = \left[\Delta x \Delta y + \frac{\Delta t^2 \Delta y g \cos\alpha}{\Delta x} \left(\sum_{k=1}^{K} H\Big|_{i,j} + \sum_{k=1}^{K} H\Big|_{i-1,j} \right) + \frac{\Delta t^2 \Delta x g \cos\alpha}{\Delta y} \left(\sum_{k=1}^{K} H\Big|_{i,j} + \sum_{k=1}^{K} H\Big|_{i,j-1} \right) \right]$$

$$S = \left[\frac{-\Delta t^2 \Delta x g \cos\alpha}{\Delta y} \sum_{k=1}^{K} H\Big|_{i,j} \right]$$

$$E = \left[\frac{-\Delta t^2 \Delta y g \cos\alpha}{\Delta x} \sum_{k=1}^{K} H\Big|_{i,j} \right]$$

$$\begin{aligned} R = {} & \Delta t \Delta y \left[\sum_{k=1}^{K} \bar{u} H_{rx}\Big|_{i,j} - \sum_{k=1}^{K} \bar{u} H_{rx}\Big|_{i-1,j} \right] + \Delta t \Delta x \left[\sum_{k=1}^{K} \bar{v} H_{ry}\Big|_{i,j} - \sum_{k=1}^{K} \bar{v} H_{ry}\Big|_{i,j-1} \right] \\ & + \Delta t^2 \Delta y \left[\sum_{k=1}^{K} F_x H_{rx}\Big|_{i,j} - \sum_{k=1}^{K} F_x H_{rx}\Big|_{i-1,j} \right] + \Delta t^2 \Delta x \left[\sum_{k=1}^{K} F_y H_{ry}\Big|_{i,j} - \sum_{k=1}^{K} F_y H_{ry}\Big|_{i,j-1} \right] \\ & - \frac{\Delta t^2 \Delta y g \cos\alpha}{\rho_\circ} \sum_{k=1}^{K} \left(\sum_{k=1}^{K} \frac{\partial \rho}{\partial x} H^2 \Big|_{i,j} - \sum_{k=1}^{K} \frac{\partial \rho}{\partial x} H^2 \Big|_{i-1,j} \right) \\ & - \frac{\Delta t^2 \Delta x g \cos\alpha}{\rho_\circ} \sum_{k=1}^{K} \left(\sum_{k=1}^{K} \frac{\partial \rho}{\partial y} H^2 \Big|_{i,j} - \sum_{k=1}^{K} \frac{\partial \rho}{\partial y} H^2 \Big|_{i,j-1} \right) \\ & + \frac{\Delta t^2 \Delta y}{\rho_\circ} \left[\left(\tau_{bx} - \tau_{sx} \right)_{i,j} - \left(\tau_{bx} - \tau_{sx} \right)_{i-1,j} \right] + \frac{\Delta t^2 \Delta x}{\rho_\circ} \left[\left(\tau_{by} - \tau_{sy} \right)_{i,j} - \left(\tau_{by} - \tau_{sy} \right)_{i,j-1} \right] \\ & + \Delta t^2 \Delta y q \left(\sum_{k=1}^{K} u_x H_{rx}\Big|_{i,j} - \sum_{k=1}^{K} u_x H_{rx}\Big|_{i-1,j} \right) + \Delta t^2 \Delta x q \left(\sum_{k=1}^{K} u_y H_{ry}\Big|_{i,j} - \sum_{k=1}^{K} u_y H_{ry}\Big|_{i,j-1} \right) \\ & - \Delta t \Delta x \Delta y q \sum_{k=1}^{K} H\Big|_{i,j} + \Delta x \Delta y n_{i,j}^{n-1} \end{aligned}$$

2.6.3 Numerical solution of the momentum equation

The X-momentum equation is solved by splitting the equation into two equations in two stages at the same time step. One of them is treated explicitly, while the second equation is treated implicitly.

Stage 1:

$$\frac{\partial \bar{u}}{\partial t} = -\bar{u}\frac{\partial \bar{u}}{\partial x} - \bar{v}\frac{\partial \bar{u}}{\partial y} - \bar{w}\frac{\partial \bar{u}}{\partial z} + g\cos\alpha\frac{\partial \eta}{\partial x} - \frac{g\cos\alpha}{\rho_\circ}\int_\eta^z \frac{\partial \rho}{\partial x}dz + f\bar{v} + g\sin\alpha$$
$$+ \frac{1}{\rho_\circ}\frac{\partial(\tau_{xx})}{\partial x} + \frac{1}{\rho_\circ}\frac{\partial(\tau_{xy})}{\partial y} + \frac{1}{\rho_\circ}\frac{\partial(\tau_{sx}+\tau_{bx})}{\partial z} + qu_x$$

Stage 2:

$$\frac{\partial \bar{u}}{\partial t} = \frac{1}{\rho_\circ}\frac{\partial(\tau_{xz})}{\partial z}$$

In the first stage, the equation is solved explicitly as follows:

$$\bar{u}^*_{i,j,k} = \bar{u}^n_{i,j,k} + \Delta t\left[\begin{array}{l} -\bar{u}\frac{\partial \bar{u}}{\partial x} - \bar{v}\frac{\partial \bar{u}}{\partial y} - \bar{w}\frac{\partial \bar{u}}{\partial z} + g\cos\alpha\frac{\partial \eta}{\partial x} - \frac{g\cos\alpha}{\rho_\circ}\int_\eta^z \frac{\partial \rho}{\partial x}dz + f\bar{v} + g\sin\alpha \\ + \frac{1}{\rho_\circ}\frac{\partial(\tau_{xx})}{\partial x} + \frac{1}{\rho_\circ}\frac{\partial(\tau_{xy})}{\partial y} + \frac{1}{\rho_\circ}\frac{\partial(\tau_{sx}+\tau_{bx})}{\partial z} + qu_x \end{array}\right]^n_{i,j,k}$$

Where: $\bar{u}^*_{i,j,k}$ represents the value of $\bar{u}_{i,j,k}$ at $t = t + \Delta t$.

The terms inside the parentheses are simplified as follows:

$$g\cos\alpha\frac{\partial \eta}{\partial x}\bigg|^n_{i,j,k} - \frac{g\cos\alpha}{\rho_\circ}\int_\eta^z \frac{\partial \rho}{\partial x}dz\bigg|^n_{i,j,k} = \frac{g\cos\alpha}{\Delta x}\left(\eta^n_{i+1,j,k} - \eta^n_{i,j,k}\right) - \frac{g\cos\alpha}{\rho\Delta x}\sum_{k=1}^{K}\left(\rho^n_{i+1,j,k} - \rho^n_{i,j,k}\right)H_{rx}\big|^n_{i,j,k}$$

$$\frac{1}{\rho_\circ}\frac{\partial(\tau_{sx}+\tau_{bx})}{\partial z}\bigg|^n_{i,j,k} = \frac{1}{\rho_\circ\Delta z}\left[\left(\tau_{sx}+\tau_{bx}\right)_{i,j,k+\frac{1}{2}} - \left(\tau_{sx}+\tau_{bx}\right)_{i,j,k-\frac{1}{2}}\right]^n$$

The remaining terms are similar to what we did in the solution of the free surface equation.

By collecting all terms, the final explicit finite difference equation of $\bar{u}^*_{i,j,k}$ will be as follows:

First we need to define [[*a*,*b*]] and ((*a*,*b*)) to be the maximum and minimum value of *a* and *b*, respectively.

$$\bar{u}^{*}_{i,j,k} = \bar{u}^{n}_{i,j,k} - \frac{\Delta t}{\Delta x}\left[\bar{u}_{i,j,k}[[\bar{u}_{i,j,k},0]] - \bar{u}_{i,j,k}((\bar{u}_{i,j,k},0)) - \bar{u}_{i-1,j,k}[[\bar{u}_{i,j,k},0]] + \bar{u}_{i+1,j,k}((\bar{u}_{i,j,k},0))\right]^{n}$$
$$- \frac{\Delta t}{\Delta y}\left[\bar{u}_{i,j,k}[[\bar{v}_{i,j,k},0]] - \bar{u}_{i,j,k}((\bar{v}_{i,j,k},0)) - \bar{u}_{i,j-1,k}[[\bar{v}_{i,j,k},0]] + \bar{u}_{i,j+1,k}((\bar{v}_{i,j,k},0))\right]^{n}$$
$$- \frac{\Delta t}{\Delta z}\left[\bar{u}_{i,j,k}[[\bar{w}_{i,j,k},0]] - \bar{u}_{i,j,k}((\bar{w}_{i,j,k},0)) - \bar{u}_{i,j-1,k}[[\bar{w}_{i,j,k},0]] + \bar{u}_{i,j+1,k}((\bar{w}_{i,j,k},0))\right]^{n}$$
$$+ \frac{\Delta t g \cos\alpha}{\Delta x}\left(\eta^{n}_{i+1,j,k} - \eta^{n}_{i,j,k}\right) - \frac{\Delta t g \cos\alpha}{\rho \Delta x}\sum_{k=1}^{K}\left(\rho^{n}_{i+1,j,k} - \rho^{n}_{i,j,k}\right)H_{rx}\Big|^{n}_{i,j,k} + \Delta t f \bar{v}^{n}_{i,j,k} + \Delta t g \sin\alpha$$
$$+ \frac{\Delta t \upsilon_h}{\Delta x_{i,j,k}}\left[\frac{\bar{u}_{i+1,j,k} - \bar{u}_{i,j,k}}{\Delta x_{i+\frac{1}{2},j,k}} - \frac{\bar{u}_{i,j,k} - \bar{u}_{i-1,j,k}}{\Delta x_{i-\frac{1}{2},j,k}}\right]^{n} + \frac{\Delta t \upsilon_h}{\Delta y_{i,j,k}}\left[\frac{\bar{u}_{i,j+1,k} - \bar{u}_{i,j,k}}{\Delta y_{i,j+\frac{1}{2},k}} - \frac{\bar{u}_{i,j,k} - \bar{u}_{i,j-1,k}}{\Delta y_{i,j-\frac{1}{2},k}}\right]^{n}$$
$$+ \frac{\Delta t}{\rho_{\circ}\Delta z}\left[\left(\tau_{sx} + \tau_{bx}\right)_{i,j,k+\frac{1}{2}} - \left(\tau_{sx} + \tau_{bx}\right)_{i,j,k-\frac{1}{2}}\right]^{n} + \Delta t q u_x\Big|^{n}_{i,j,k}$$

Now, $\bar{u}^{*}_{i,j,k}$ is calculated at each cell face and will be used to calculate $\bar{u}^{n+1}_{i,j,k}$ by solving the second equation implicitly.

In the second stage, the equation is solved by using a fully implicit finite difference technique for the vertical diffusion term as follows:

$$\frac{\partial \bar{u}}{\partial t} = \frac{\partial}{\partial z}\left[\upsilon_v \frac{\partial \bar{u}}{\partial z}\right]$$

$$\frac{\bar{u}^{n+1}_{i,j,k} - \bar{u}^{*}_{i,j,k}}{\Delta t} = \frac{1}{\Delta z_{i,j,k}}\left[\upsilon_{v_{i,j,k}}\frac{\bar{u}^{n+1}_{i,j,k+1} - \bar{u}^{n+1}_{i,j,k}}{\Delta z_{i,j,k+\frac{1}{2},k}} - \upsilon_{v_{i,j,k-1}}\frac{\bar{u}^{n+1}_{i,j,k} - \bar{u}^{n+1}_{i,j,k-1}}{\Delta z_{i,j,k-\frac{1}{2},k}}\right]$$

$$\bar{u}^{n+1}_{i,j,k} = \bar{u}^{*}_{i,j,k} + \frac{\Delta t}{\Delta z_{i,j,k}}\left[\upsilon_{v_{i,j,k}}\frac{\bar{u}^{n+1}_{i,j,k+1} - \bar{u}^{n+1}_{i,j,k}}{\Delta z_{i,j,k+\frac{1}{2}}} - \upsilon_{v_{i,j,k-1}}\frac{\bar{u}^{n+1}_{i,j,k} - \bar{u}^{n+1}_{i,j,k-1}}{\Delta z_{i,j,k-\frac{1}{2}}}\right]$$

$$\left[-\frac{\Delta t \upsilon_{v_{i,j,k-1}}}{\Delta z_{i,j,k}\Delta z_{i,j,k-\frac{1}{2}}}\right]\bar{u}^{n+1}_{i,j,k-1} + \left[1 + \frac{\Delta t \upsilon_{v_{i,j,k-1}}}{\Delta z_{i,j,k}\Delta z_{i,j,k+\frac{1}{2}}} + \frac{\Delta t \upsilon_{v_{i,j,k}}}{\Delta z_{i,j,k}\Delta z_{i,j,k-\frac{1}{2}}}\right]\bar{u}^{n+1}_{i,j,k}$$
$$+ \left[-\frac{\Delta t \upsilon_{v_{i,j,k}}}{\Delta z_{i,j,k}\Delta z_{i,j,k+\frac{1}{2}}}\right]\bar{u}^{n+1}_{i,j,k+1} = \bar{u}^{*}_{i,j,k}$$

For more simplification, the above equation can be written as follows:

$$U\bar{u}^{n+1}_{i,j,k-1} + C\bar{u}^{n+1}_{i,j,k} + D\bar{u}^{n+1}_{i,j,k+1} = R$$

Where:

$$U = \left[-\frac{\Delta t \upsilon_{v_{i,j,k-1}}}{\Delta z_{i,j,k} \Delta z_{i,j,k-½}} \right]$$

$$C = \left[1 + \frac{\Delta t \upsilon_{v_{i,j,k-1}}}{\Delta z_{i,j,k} \Delta z_{i,j,k+½}} + \frac{\Delta t \upsilon_{v_{i,j,k}}}{\Delta z_{i,j,k} \Delta z_{i,j,k-½}} \right]$$

$$D = \left[-\frac{\Delta t \upsilon_{v_{i,j,k}}}{\Delta z_{i,j,k} \Delta z_{i,j,k+½}} \right]$$

$$R = \bar{u}^{*}_{i,j,k}$$

A system of linear algebraic equations for each line or column in the domain is solved by using Thomas algorithm to calculate $\bar{u}^{n+1}_{i,j,k}$ at the center of each cell face perpendicular to x-direction. A similar procedure is used to solve Y-momentum equation.

2.6.4 Numerical solution of the continuity equation

After calculated $\bar{u}^{n+1}_{i,j,k}$ and $\bar{v}^{n+1}_{i,j,k}$, the vertical velocity component $\bar{w}^{n+1}_{i,j,k}$ can be calculated from the continuity equation by implementing the cell by cell calculations and as follows:

$$\frac{\partial \bar{u}}{\partial x} + \frac{\partial \bar{v}}{\partial y} + \frac{\partial \bar{w}}{\partial z} = 0$$

$$\frac{\bar{u}^{n+1}_{i,j,k} - \bar{u}^{n+1}_{i-1,j,k}}{\Delta x} + \frac{\bar{v}^{n+1}_{i,j,k} - \bar{v}^{n+1}_{i,j-1,k}}{\Delta y} + \frac{\bar{w}^{n+1}_{i,j,k} - \bar{w}^{n+1}_{i,j,k-1}}{\Delta z} = 0$$

$$\bar{w}^{n+1}_{i,j,k-1} = \bar{w}^{n+1}_{i,j,k} + \frac{\bar{u}^{n+1}_{i,j,k} - \bar{u}^{n+1}_{i-1,j,k}}{\Delta x} \Delta z + \frac{\bar{v}^{n+1}_{i,j,k} - \bar{v}^{n+1}_{i,j-1,k}}{\Delta y} \Delta z$$

2.6.5 Numerical solution of heat and water quality transport equation

The water quality transport equation is

$$\frac{\partial \phi}{\partial t} + \frac{\partial \bar{u} \phi}{\partial x} + \frac{\partial \bar{v} \phi}{\partial y} + \frac{\partial \bar{w} \phi}{\partial z} = \frac{\partial}{\partial x}\left[D_h \frac{\partial \phi}{\partial x} \right] + \frac{\partial}{\partial y}\left[D_h \frac{\partial \phi}{\partial y} \right] + \frac{\partial}{\partial z}\left[D_v \frac{\partial \phi}{\partial z} \right] + S_\phi$$

This equation is also splitting into two equations in two stages at the same time step. In the first stage, the equation is treated explicitly by implementing the upwind difference scheme for advective terms and a fully explicit scheme for the horizontal diffusion terms and source/sink

term. In the second equation, the equation is treated implicitly by implementing a fully implicit scheme for the vertical diffusion term:

Stage 1:

$$\frac{\partial \phi}{\partial t}+\frac{\partial \bar{u}\phi}{\partial x}+\frac{\partial \bar{v}\phi}{\partial y}=\frac{\partial}{\partial x}\left[D_h\frac{\partial \phi}{\partial x}\right]+\frac{\partial}{\partial y}\left[D_h\frac{\partial \phi}{\partial y}\right]+S_\phi$$

Stage 2:

$$\frac{\partial \phi}{\partial t}+\frac{\partial \bar{w}\phi}{\partial z}=\frac{\partial}{\partial z}\left[D_v\frac{\partial \phi}{\partial z}\right]$$

The finite difference formulation of the first stage is as follows:

$$\begin{aligned}adv\big|_{i,j,k}^{n}=&\frac{1}{\Delta x_{i,j,k}}\left[\phi_{i,j,k}[[\bar{u}_{i,j,k},0]]-\phi_{i,j,k}((\bar{u}_{i,j,k},0))-\phi_{i-1,j,k}[[\bar{u}_{i,j,k},0]]+\phi_{i+1,j,k}((\bar{u}_{i,j,k},0))\right]^n\\&+\frac{1}{\Delta y_{i,j,k}}\left[\phi_{i,j,k}[[\bar{v}_{i,j,k},0]]-\phi_{i,j,k}((\bar{v}_{i,j,k},0))-\phi_{i-1,j,k}[[\bar{v}_{i,j,k},0]]+\phi_{i+1,j,k}((\bar{v}_{i,j,k},0))\right]^n\\&+\frac{1}{\Delta z_{i,j,k}}\left[\phi_{i,j,k}[[\bar{w}_{i,j,k},0]]-\phi_{i,j,k}((\bar{w}_{i,j,k},0))-\phi_{i,j,k-1}[[\bar{w}_{i,j,k},0]]+\phi_{i,j,k+1}((\bar{w}_{i,j,k},0))\right]^n\end{aligned}$$

$$diff\big|_{i,j,k}^{n}=\frac{D_h}{\Delta x_{i,j,k}}\left[\frac{\phi_{i+1,j,k}-\phi_{i,j,k}}{\Delta x_{i+\frac{1}{2},j,k}}-\frac{\phi_{i,j,k}-\phi_{i-1,j,k}}{\Delta x_{i-\frac{1}{2},j,k}}\right]^n+\frac{D_h}{\Delta y_{i,j,k}}\left[\frac{\phi_{i,j+1,k}-\phi_{i,j,k}}{\Delta y_{i,j+\frac{1}{2},k}}-\frac{\phi_{i,j,k}-\phi_{i,j-1,k}}{\Delta y_{i,j-\frac{1}{2},k}}\right]^n$$

$$\phi\big|_{i,j,k}^{*}=\phi\big|_{i,j,k}^{n}+\Delta t\left(-adv\big|_{i,j,k}^{n}+diff\big|_{i,j,k}^{n}+S_\phi\big|_{i,j,k}^{n}\right)$$

Also, the finite difference formulation of the second stage is as follows:

$$\frac{\phi\big|_{i,j,k}^{n+1}-\phi\big|_{i,j,k}^{*}}{\Delta t}=\frac{1}{\Delta z_{i,j,k}}\left[D_{vi,j,k}\frac{\phi_{i,j,k+1}-\phi_{i,j,k}}{\Delta z_{i,j,k+\frac{1}{2}}}-D_{vi,j,k-1}\frac{\phi_{i,j,k}-\phi_{i,j,k-1}}{\Delta z_{i,j,k-\frac{1}{2}}}\right]^{n+1}$$

$$\left[-\frac{\Delta tD_{vi,j,k-1}}{\Delta z_{i,j,k}\Delta z_{i,j,k-\frac{1}{2}}}\right]\phi_{i,j,k-1}^{n+1}+\left[1+\frac{\Delta tD_{vi,j,k}}{\Delta z_{i,j,k}\Delta z_{i,j,k+\frac{1}{2}}}+\frac{\Delta tD_{vi,j,k-1}}{\Delta z_{i,j,k}\Delta z_{i,j,k-\frac{1}{2}}}\right]\phi_{i,j,k}^{n+1}+\left[-\frac{\Delta tD_{vi,j,k}}{\Delta z_{i,j,k}\Delta z_{i,j,k+\frac{1}{2}}}\right]\phi_{i,j,k+1}^{n+1}=\phi_{i,j,k}^{*}$$

For more simplification, the above equation can be written as follows:

$$U\phi_{i,j,k-1}^{n+1}+C\phi_{i,j,k}^{n+1}+D\phi_{i,j,k+1}^{n+1}=R$$

Where:

$$U=\left[-\frac{\Delta tD_{vi,j,k-1}}{\Delta z_{i,j,k}\Delta z_{i,j,k-\frac{1}{2}}}\right]$$

$$C = \left[1 + \frac{\Delta t D_{vi,j,k}}{\Delta z_{i,j,k} \Delta z_{i,j,k+½}} + \frac{\Delta t D_{vi,j,k-1}}{\Delta z_{i,j,k} \Delta z_{i,j,k-½}} \right]$$

$$D = \left[- \frac{\Delta t D_{vi,j,k}}{\Delta z_{i,j,k} \Delta z_{i,j,k+½}} \right]$$

$$R = \phi^{*}_{i,j,k}$$

2.7 Model verification:

In a first step after developing of the numerical model and before proceeding further to add more features or applying the model to a real case, it is necessary to test the model in order to determine its validity. The verification of the model was done by comparing model predictions to known solutions test cases. The model results were also tested by doing volume balance analysis.

2.7.1 Test 1: Free surface seiching in a closed rectangular basin

This test was done in a similar way to that test recommended by Wang, S.Y. and Roache, P.J. and Schmalz, R.A. and Jia, Y. and Smith (2009). A closed rectangular basin is subjected to an initial vertical displacement in which the free surface wave has a profile of half cosine in the longitudinal direction as shown in Figure 6.

The basin dimensions are:

L=38000m

B=6000m

H=12m

The initial vertical amplitude at the left and right boundaries of the basin, $\eta_{\circ}$, is 25cm.

Thus, after releasing the system from the rest, the oscillated wave starts and continues with time. If there were a frictional resistance, the wave is damped and eventually the system goes to the rest.

Assumptions:

- The closed boundaries are frictionless (no-slip boundaries).
- Neglected top and bottom shear stresses.

- Neglected advection and diffusion terms.
- The fluid is viscousless and has a constant density, ρ=1000kg/m^3.
- Neglected Coriolis force, f =0.
- Hydrostatic pressure.
- Boussinesq approximations.
- No source/sink.

Analytical solution:

Based on the above assumptions, the simple one-dimensional governing equations can be written as follows:

Free surface equation:

$$\frac{\partial \eta}{\partial t} + \frac{\partial uH}{\partial x} = 0$$

X-momentum equation:

$$\frac{\partial u}{\partial t} + g\frac{\partial \eta}{\partial x} = 0$$

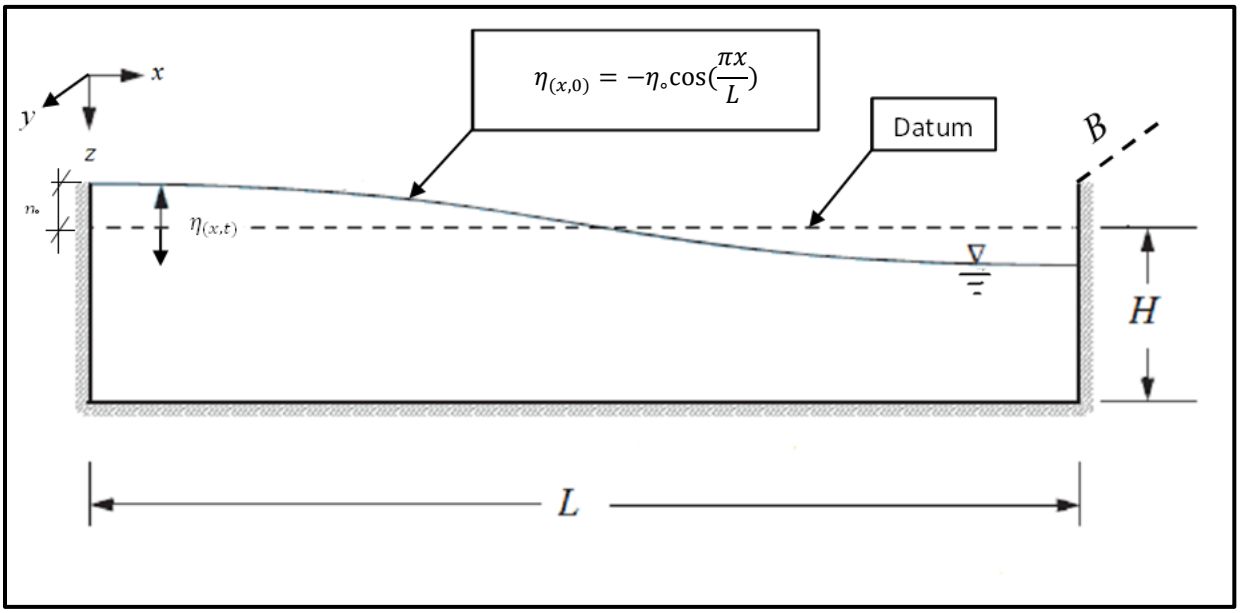

Figure 6: Seiching basin for the test 1

Thus, the analytical solutions is given by Eliason and Bourgeois (1997) :

$$\eta_{(x,t)} = \eta_{\circ} \cos\left(\frac{\pi x}{L}\right) \cos(\frac{\pi\sqrt{gH}}{L} t)$$

$$u_{(x,t)} = \frac{\eta_{\circ}\sqrt{gH}}{H} \sin\left(\frac{\pi x}{L}\right) \sin(\frac{\pi\sqrt{gH}}{L} t)$$

Where $\sqrt{gH}$ is the gravity wave speed.

Initial conditions:

$\eta_{(x,0)} = -0.25 \times \cos(\frac{\pi x}{L})$

$u = v = w = 0$

Boundary conditions:

No-slip boundary conditions are applied along the closed boundary ($u = v = w = 0$) in additional to the following Neumann boundary conditions:

- Boundaries normal to the x-axis, $\frac{\partial v}{\partial x} = \frac{\partial \eta}{\partial x} = 0$
- Boundaries normal to the y-axis, $\frac{\partial u}{\partial y} = \frac{\partial \eta}{\partial y} = 0$
- Boundaries normal to the z-axis, $\frac{\partial u}{\partial z} = \frac{\partial v}{\partial z} = 0$

The domain is divided into total computational cells of 1575 (21×5×15), in which *kt*=3 and internal cells of 684. The size of the computational cells is $\Delta x = \Delta y = 2000m$ and $\Delta z = 1m$. The advection and diffusion terms, top and bottom shear stresses, and Coriolis force were set to zero in the model to agree with the analytical solution. To maintain a stable solution, the time step should be satisfied the stability condition which is the gravity courant number must be less than or equal to unity ($\frac{\sqrt{gH}\Delta t}{\Delta x} \leq 1$). Thus, we proposed using time step of $\Delta t = 100, 70, 50, and\ 5\ sec$ to guarantee the stability for the comparison purpose with analytical solution.

A comparison in the water level (η) and longitudinal velocity (u) between the model results and the analytical solution for the seiching basin was done. In Figures 7,8,9, and 10, the comparison was done near the left and right boundary of the basin where the wave amplitude is high enough to see. The distance between the selected left location and the nearest boundary is equal to the distance between the selected right location and its nearest boundary, i.e. symmetric locations. This helps to ensure that if the solution were correct, the two waves at these locations would

have opposite direction and same magnitude at the same time of simulation. The results show that a good agreement with the following the analytical solution signal even though there is damping of the numerical solution. The damping is arising from using the implicit technique in the solution of the free surface equation (Vreugdenhil 1989). The implicit scheme helps getting rid of the celerity stability condition (Wells 1999), however it has wave damping. Figure 11 shows the effect of time step on wave damping. By reducing the time step, the damping decreases. This agree with Vreugdenhil (1989) in that "the time step is the major factor influencing the accuracy". Another aspect here is that the numerical solution is following the analytical solution without phase lag and for any time step within the stability region; therefore, no phase error that affects the accuracy is produced. Wells (1999) showed that running the model with a high time step reduces the accuracy, however evaluating the time step by doing sensitivity analysis helps in choosing an appropriate time step.

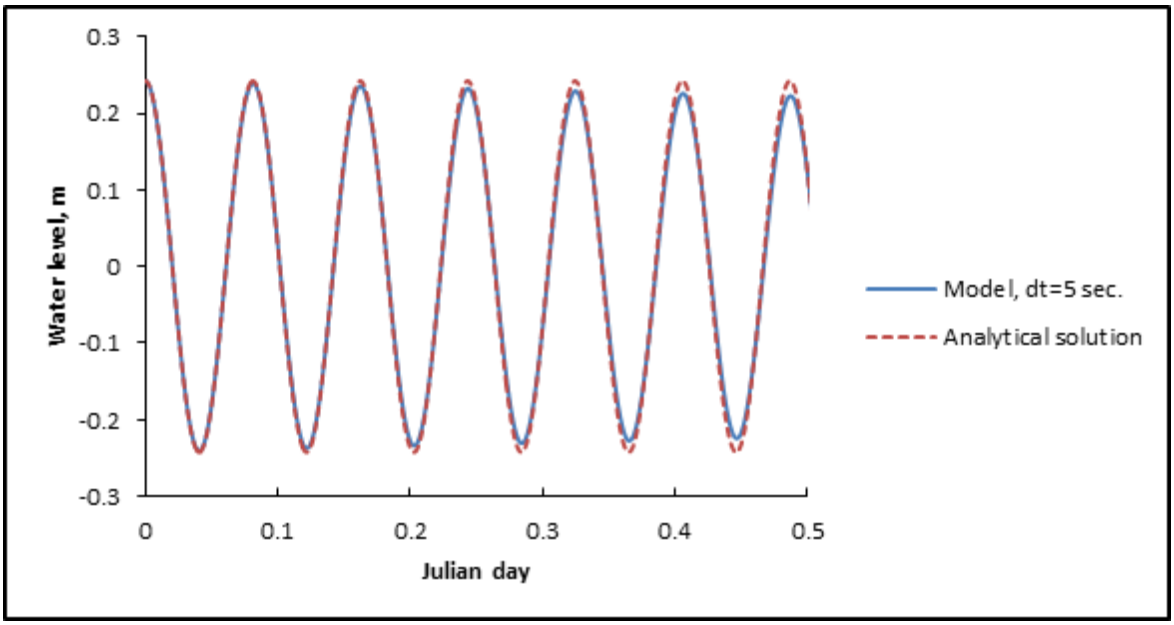

Figure 7: Comparison in the water level (η) between the model results and the analytical solution for the seiching basin near the right boundary (i=19, j=3, and k=kt=3), Δt=5 sec

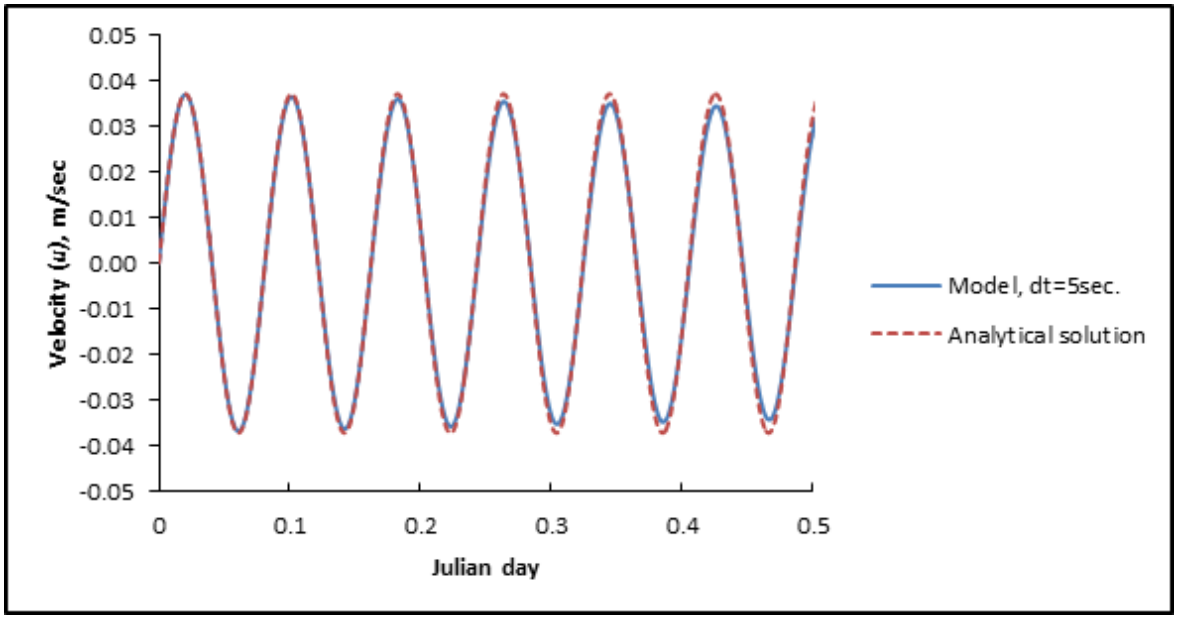

Figure 8: Comparison in the longitudinal velocity (u) between the model results and the analytical solution for the seiching basin near the right boundary (i=19, j=3, and k=kt=3), Δt=5 sec

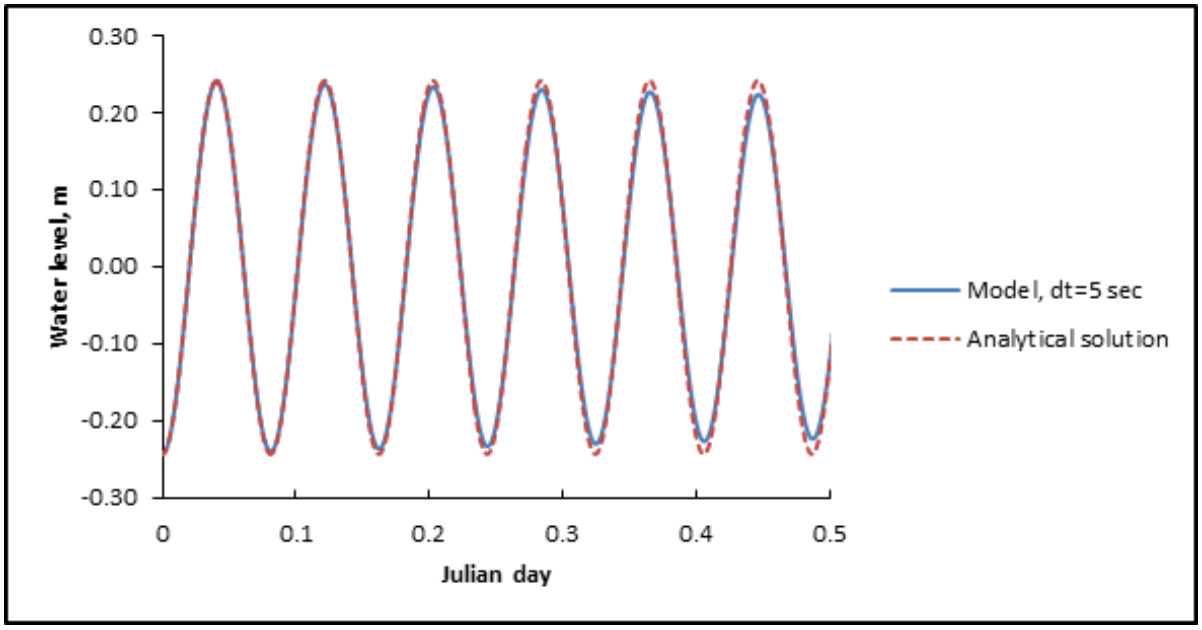

Figure 9: Comparison in the water level (η) between the model results and the analytical solution for the seiching basin near the left boundary (i=3, j=3, and k=kt=3), Δt=5 sec

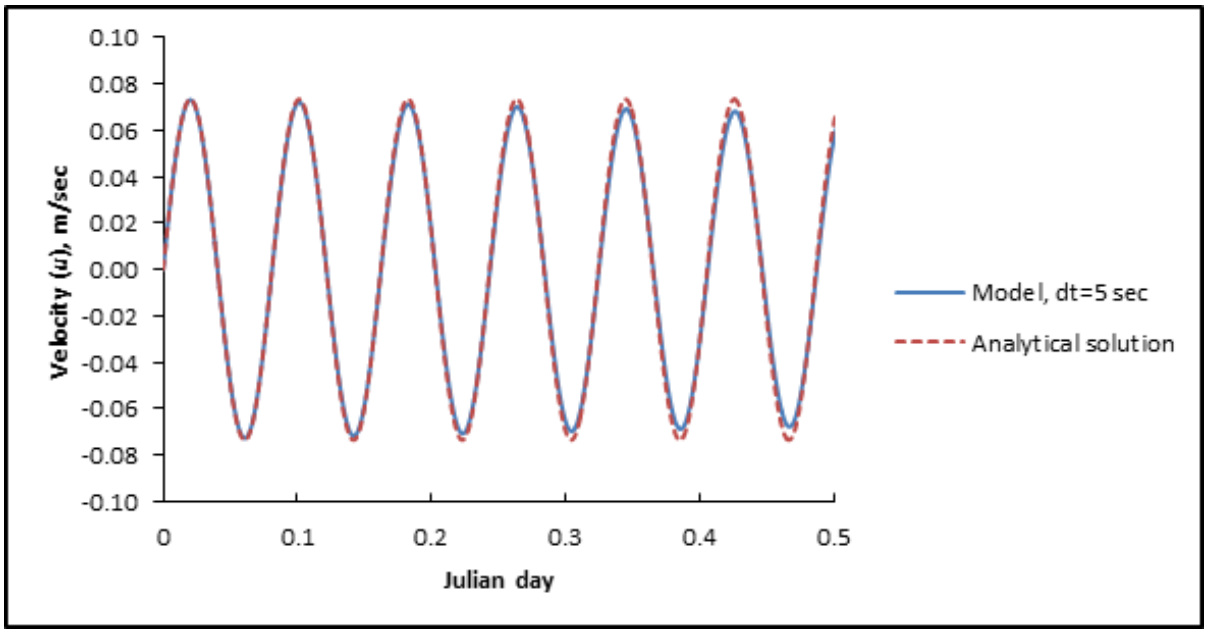

Figure 10: Comparison in the longitudinal velocity (u) between the model results and the analytical solution for the seiching basin near the left boundary (i=3, j=3, and k=kt=3), Δt=5 sec

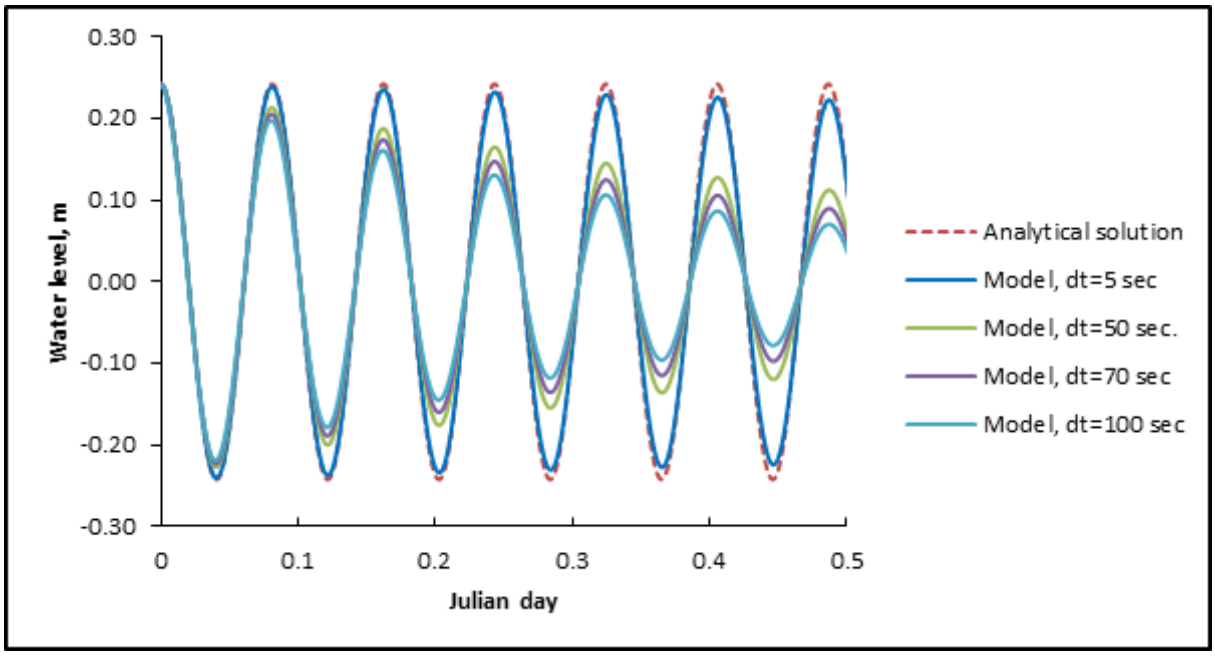

Figure 11: Dumping effect on the computed water level wave using different time steps for the seiching basin near the right boundary (*i*=19, *j*=3, and *k*=*kt*=3)

2.7.2 Test 2: Free water surface response to wind-induced flow in a closed rectangular basin

To evaluate the influence of the wind shear stress τ_s on the numerical solution in test case 1, we added the surface shear stress to X-momentum equation that governs the seiching basin. Then the governing equations of this test are:

Free surface equation:

$$\frac{\partial \eta}{\partial t} + \frac{\partial uH}{\partial x} = 0$$

X-momentum equation:

$$\frac{\partial u}{\partial t} + g\frac{\partial \eta}{\partial x} = \frac{\tau_s}{\rho_\circ H}$$

If we considered $x = 0$ is at the center of the basin as shown in Figure 12, in which $L = 2b$, and suddenly a constant wind W starts hitting the flat water surface, $\eta = 0$, in the positive x-direction and continues blowing with time, the analytical solution for the water elevation is as follows (Wells 1999):

$$\eta_{(x,t)} = \frac{u_*^2}{gH}x - \frac{8bu_*^2}{\pi^2 gH}\left[\cos\left(\frac{\pi\sqrt{gH}t}{2b}\right)\sin\left(\frac{\pi x}{2b}\right) - \frac{1}{9}\cos\left(\frac{3\pi\sqrt{gH}t}{2b}\right)\sin\left(\frac{3\pi x}{2b}\right) + \frac{1}{25}\cos\left(\frac{5\pi\sqrt{gH}t}{2b}\right)\sin\left(\frac{5\pi x}{2b}\right) - \cdots\right]$$

Where u_* is the surface shear velocity.

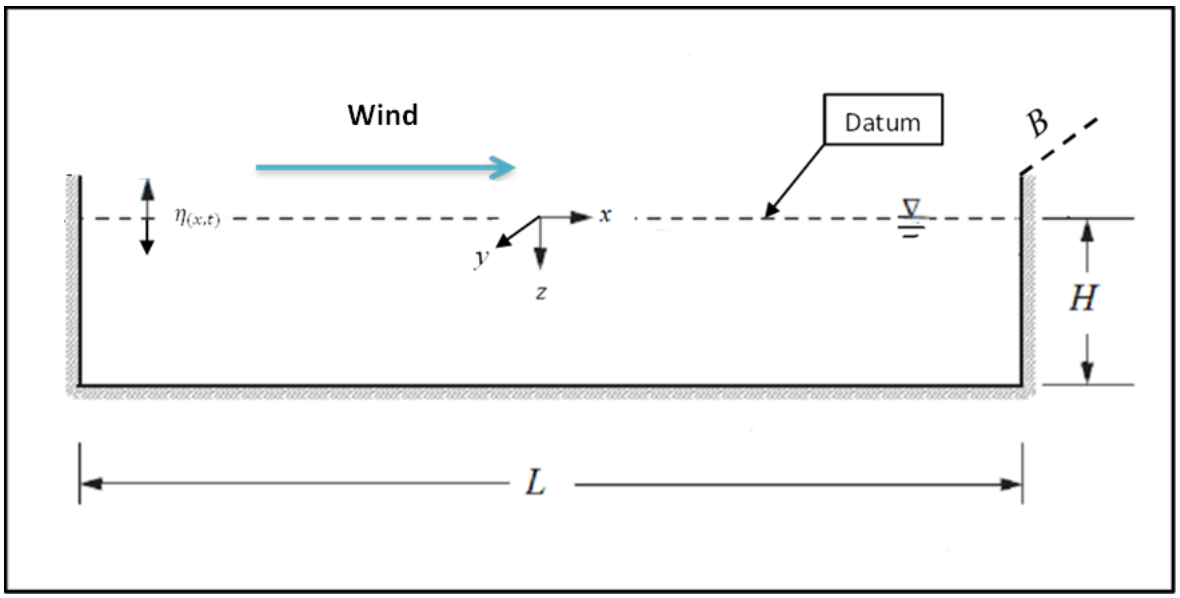

Figure 12: Seiching basin for the test 2

The code of test case 1 was run with a constant wind of 2*m*/*sec* at 10*m* height above the water surface at $t = 0$. A comparison in the water level (η) between the model results and the analytical solution near the left boundary of the seiching basin was shown in in Figure 13. The model gives good results in following the surface wave signal of the analytical solution with a behavior similar to that in test case 1. Therefore, we could say that under the effect of wind there in no extra damping to the surface wave comparing to case where there is no wind. Figure 14 shows the wind effect on the water surface level upstream and downstream of the basin. In this case there are waves of opposite directions at both left and right end similar to those of test case 1, but here the upstream wave has positive amplitude which is less than the negative amplitude of the downstream wave, implying the water surface has a positive slope in the wind direction. Thus, this confirms the good agreement of the model to the basic theories of transporting the one-dimensional water surface waves under the influence of wind.

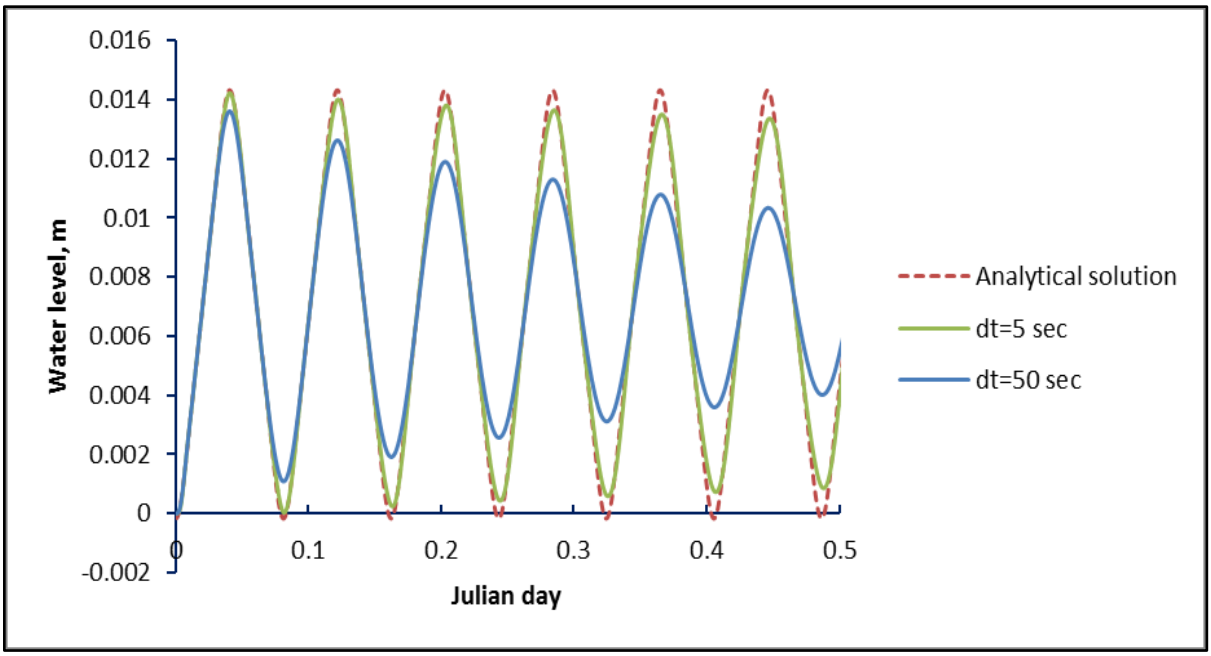

Figure 13: The computed water level under the wind effect in a closed rectangular basin using different time steps for the seiching basin near the left boundary (*i*=3, *j*=3, and *k*=*kt*=3)

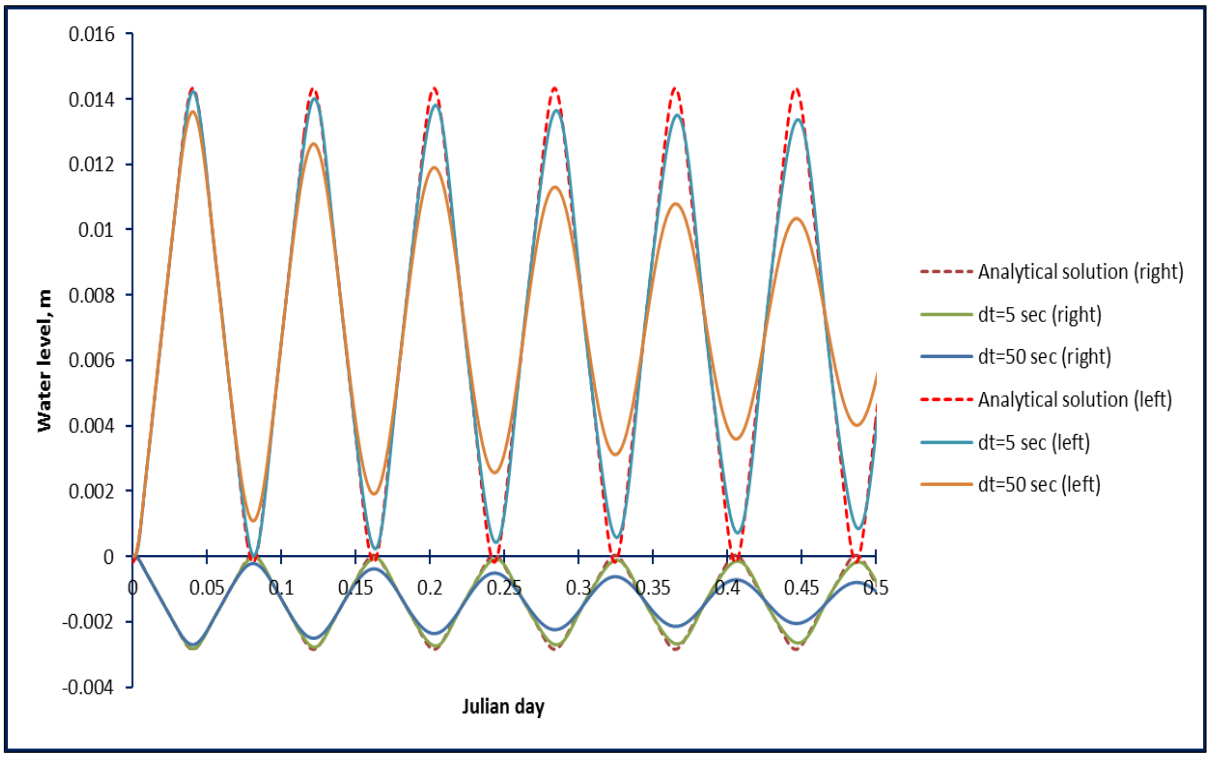

Figure 14: The computed water level under the wind effect in a closed rectangular basin using different time steps for the seiching basin near the left and right boundaries (*i*=3 and *i*=19, *j*=3, and *k*=*kt*=3)

2.7.3 Test 3: Velocity profile response to the wind induced flow in a closed rectangular basin

The surface shear stresses due to the wind blowing on the water body transfer vertically resulting in a velocity profile in which the water surface flows in the direction of the wind downstream and then it hits the boundary and circulates back upstream through the bottom layers. Different models are available to represent the analytical velocity profile. One of these models is a model developed by (Hansen 1975). The analytical solution is in term of error function and as follows:

$$\frac{u}{u_*} = 6.65\left[1 - \text{erf}(\frac{z}{0.267u_*t})\right]$$

Where *u* is the longitudinal velocity over time at a depth of *z* below the water surface, see Figure 15.

Since the solution is based on assuming there is a balance between the rate of change of the longitudinal velocity and its vertical diffusion only, we need to run the code for a short period of time when the change in the water surface level can be considered negligible to agree with the analytical solution. Also, we need to turn off the horizontal advection, horizontal diffusion, and Coriolis force. Using a constant vertical eddy viscosity over depth $v_t = \frac{1}{28}u_*t$ (Wells 1999) and wind of 10*m*/*sec* in the positive x-direction, the code was run for 1000sec. Figure 16 shows the computed and analytical velocity profile under the effect of wind induced flow in the middle of the seiching basin where the effect of circulation and boundaries are negligible. The model gave a very good agreement with the analytical solution.

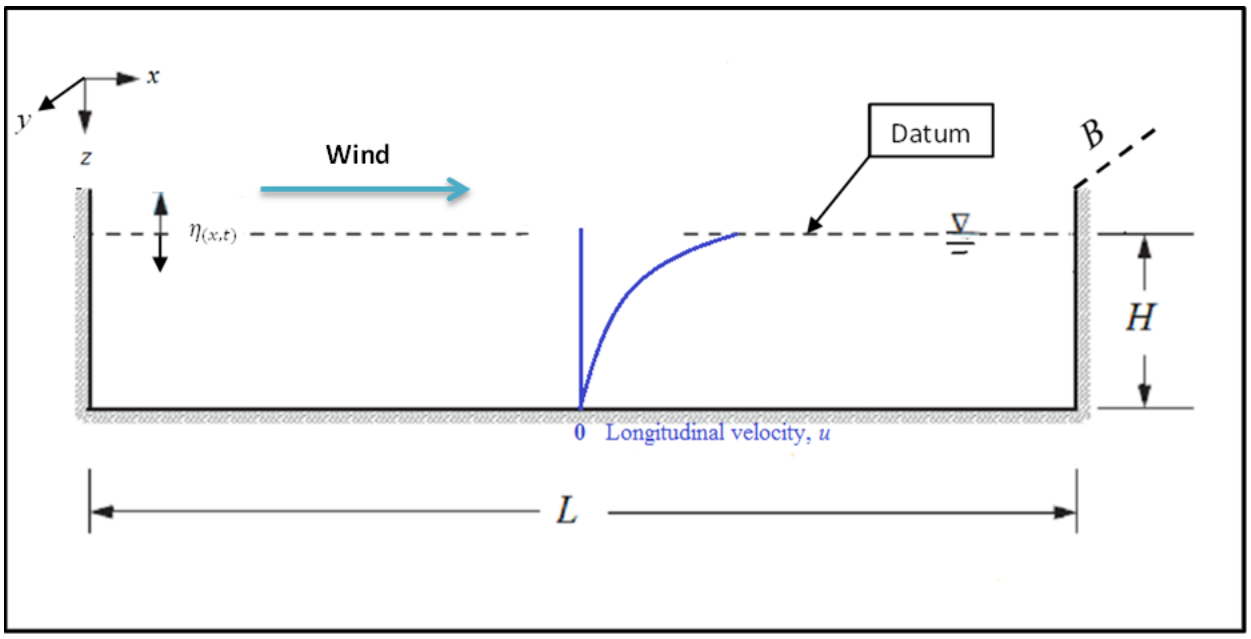

Figure 15: Seiching basin for the test 3

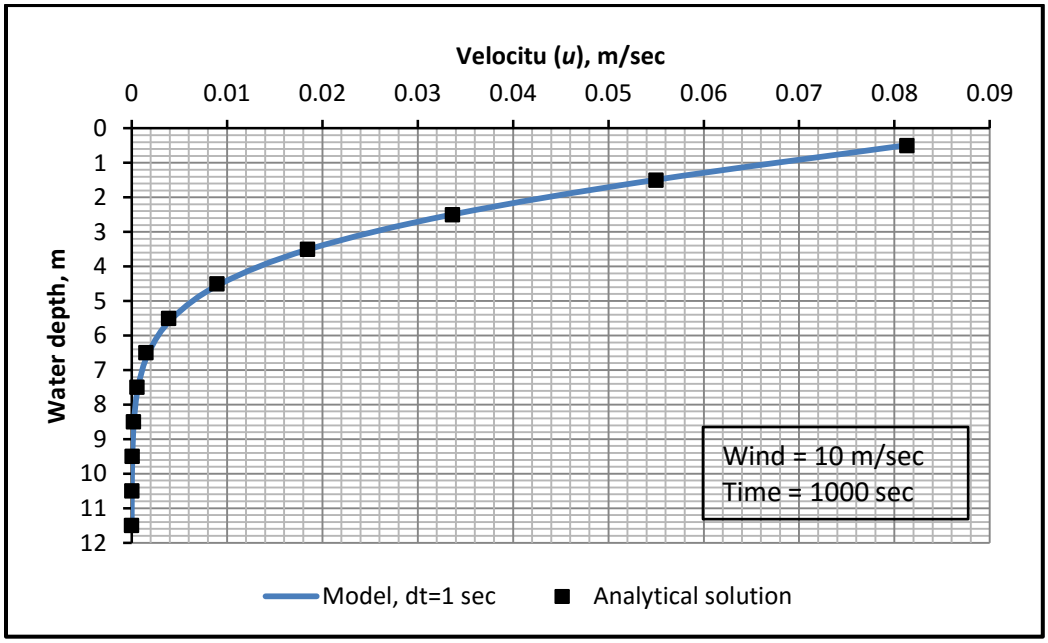

Figure 16: The computed and analytical velocity profile under the effect of wind induced flow in the middle of the seiching basin at time = 1000sec

3 CONCLUSIONS

In order to validate and verified the numerical model, comparisons between the numerical and analytical solution were done. This is the first step after developing any numerical model and before proceeding further to add more features or applying the model to real test cases. The model should satisfy the analytical solution as close as possible because of model is based on finite differences which are an approximation to the analytical solution. The model showed good agreement with the analytical solution for free surface seiching in a closed rectangular basin, free water surface response to wind-induced flow in a closed rectangular basin, and velocity profile response to the wind induced flow in a closed rectangular basin. Even though the model showed a stable solution within the stability region, the low time step showed a better match with the analytical solution than the higher time step. Thus, modelers should check the model behavior as a function of time step. Hence, even though a model is stable, one still needs to evaluate model error by time step refinement.

4 REFERENCES

Ahsan, A.K.M.Q., and Blumberg, A.F., 1999. Three-Dimensional Hydrothermal Model of Onondaga Lake, New York. *Journal of Hydraulic Engineering*, 125(9), pp.912–923.

Blumberg, A.F., and Mellor, G.L., 1987. A description of a three-dimensional coastal ocean circulation model. *Three-dimensional coastal ocean models. N. S. Heaps, ed., American Geophysical Union, Washington, D.C.*, 4, pp.1–16.

Bryan, K., 1969. A numerical method for the study of the circulation of the world ocean. *Journal of Computational Physics*, 4(3), pp.347–376. Available at: http://www.sciencedirect.com/science/article/pii/0021999169900047.

Buchak, E., and Cole, T., 1995. CE-QUAL-W2: A Two-Dimensional, Laterally Averaged, Hydrodynamic and Water Quality Model, Version 2.0. User Manual. *Instruction Rep. EL-95-1, U.S. Army Corps of Engineers, Washington, D.C.*

Casulli, V., and Cheng, R.T., 1992. Semi-implicit finite difference methods for three-dimensional shallow water flow. *International Journal for Numerical Methods in Fluids*, 15(6), pp.629–648.

Casulli, V., and Walters, R., 2000. An unstructured grid, three-dimensional model based on the shallow water equations. *International Journal for Numerical Methods in Fluids*, 32, pp.331–348. Available at: http://eportfolio.lib.ksu.edu.tw/~T097000001/repository/fetch/Casulli2000.pdf.

Eliason, D.E., and Bourgeois, A.J., 1997. Validation of numerical shallow water models for stratified seiches. *International Journal for Numerical Methods in Fluids*, 24(8), pp.771–786. Available at: http://www.scopus.com/inward/record.url?eid=2-s2.0-0031126669&partnerID=40&md5=3a7aee5cb35d5d7576b253b699e7bc8d.

Fofonoff, N.P., 1962. Physical properties of seawater. In *The Sea, Ideas and Observations on Progress in the Study of the Seas: Physical oceanography*. Vol. 1, M. N. Hill, ed., Wiley Interscience, New York, pp. 3–30. Available at: https://books.google.com/books/about/The_Sea_Ideas_and_Observations_on_Progre.html?i

d=P7xRAAAAMAAJ&pgis=1 [Accessed June 29, 2015].

Hamrick, J.M., 1992. A Three-Dimensional Environmental Fluid Dynamics Computer Code: Theoretical and Computational Aspects. *The College of William and Mary, Virginia Institute of Marine Science. Special Report 317, 63 pp.*

Hansen, N.E., 1975. Entrainment in Two-Layered Flows, Institute of Hydrodynamics and Hydraulic Engineering. *Technical Institute of Denmark, Series Paper No. 7.*

Hodges, B., and Dallimore, C., 2006. Estuary , Lake and Coastal Ocean Model : ELCOM v2 . 2 Science Manual. *Center for Water Research, University of Western Australia*, p.62.

Mellor, G.L., 2003. Users guide for a three-dimensional, primitive equation, numerical ocean model (June 2003 version). *Prog. in Atmos. and Ocean. Sci, Princeton University*, (October), p.53.

Mellor, G.L., and Yamada, T., 1982. Development of a turbulence closure model for geophysical fluid problems. *Reviews of Geophysics*, 20(4), p.851.

Smagorinsky, J., 1963. General circulation experiments wiht the primitive equations I. The basic experiment. *Monthly Weather Review*, 91(3), pp.99–164.

Smith, P.E., 2006. A Semi-Implicit , Three-Dimensional Model for Estuarine Circulation. *U.S. Geological Survey Open-File Report 2006–1004, 176 p.*

Tetra Tech, I., 2002. Draft user's manual for environmental fluid dynamic code Hydro Version (EFDC-Hydro) Release 1.00. *Tetra Tech, Inc., Fairfax, Virginia*.

Vreugdenhil, C.B., 1989. Computational Hydraulics An Introduction. *Springer-Verlag Berlin Heidelberg*.

Wang, H., and Falconer, R.A., 1998. Numerical modeling of flow in chlorine disinfection tank. *Journal of Hydraulic Engineering*, 124(9), pp.918–931.

Wang, S.Y. and Roache, P.J. and Schmalz, R.A. and Jia, Y. and Smith, P.E., 2009. Verification and Validation of 3D Free-Surface Flow Models.

Wells, S.A., 1999. Basis for the CE-QUAL-W2 version 3 river basin hydrodynamic and water quality model. *ASCE International Water Resources Engineering Conference*, pp.1–11.